Maximum entropy model reveals frequent brain state switching in a multiversal brain function analysis in early psychoses

Nicholas Theis[1], Jonathan Rubin[2], Ella O'Rourke[1], Jyotika Bahuguna[3], Joshua Cape[4], Bowei Ouyang[1], Satish Iyengar[5], Konasale M. Prasad[1,6,7*]

[1]Department of Psychiatry, University of Pittsburgh School of Medicine, Pittsburgh, PA 15213

[2]Department of Mathematics, University of Pittsburgh Kenneth Deitrich School of Arts and Sciences, Pittsburgh, PA 15213

[3]Department of Neuroscience, Laboratoire de Neurosciences Cognitive et Adaptive, University of Strasbourg, Strasbourg, France

[4]Department of Statistics, University of Wisconsin, Madison, Wisconsin

[5]Department of Statistics, University of Pittsburgh Kenneth Deitrich School of Arts and Sciences, Pittsburgh, PA 15213

[6]Department of Bioengineering, Swanson School of Engineering, University of Pittsburgh, Pittsburgh PA 15213

[7]VA Pittsburgh Healthcare System, Pittsburgh, PA 15240

***Corresponding author:**
Western Psychiatric Institute and Clinic
3811 O'Hara Street
Pittsburgh, PA 15213, USA
KMP8@pitt.edu

Abstract

Background: Regional activation and pairwise correlation are mainstay neuroimaging methods. Yet, neither approach fully captures brain networks' temporal evolution and interaction. The maximum entropy model (MEM), which integrates regional and inter-regional activity, represents a promising integrative approach to examine dynamically evolving functional networks.

Methods: Activation-only, pairwise-coactivation-only, and MEM-based analyses were applied to the Human Connectome Project-Early Psychosis dataset (patients=109, controls=56). Using the HCP/Glasser atlas to define brain regions from the default mode (DMN) and dorsal attention (DAN) networks, group differences were quantified in nodal frequency band power, functional connectivity (FC), and MEM features such as transition rates between basins in energy landscapes and their associations with cognitive and psychopathological measures.

Results: Psychosis was associated with reduced BOLD frequency band power and FC graph metrics. The MEM demonstrated a variety of DMN and DAN nodal activation/deactivation patterns, with more frequent switching between them during the resting state in psychosis. Higher basin transitions with reduced basin dwell times were observed in DMN and DAN nodes, more prominently in DMN+DAN system. BOLD frequency band power of three regions correlated positively with working memory, but FC graph metrics did not. MEM metrics correlated negatively with working memory and positively with positive symptom severity.

Conclusion: The MEM provides unique information unavailable from the other two methods, namely nodal activation/deactivation patterns, basin transitions, and energy. Network-level results were better characterized in the MEM analysis as attenuated inter-network connectivity with reduced stability of DMN and DAN in psychosis that may underlie impaired working memory and psychopathology severity.

Key Words: fMRI; Dynamical system; functional connectivity; frequency band power; default mode network; dorsal attention network; psychosis

Introduction

Brain network dysconnectivity is proposed to underlie psychotic disorders(1). Functional magnetic resonance imaging (fMRI)-based studies have reported several important findings in psychosis(2-5) with considerable variability(6). A "multiversal" approach (concurrent application of complementary methods within a sample)(7), can reduce such variability and improve interpretability(8,9). We examined the nodal activity in the blood oxygenation level dependent (BOLD) signal in the frequency domain, inter-nodal functional connectivity (FC), and systems-level maximum entropy model (MEM)-based features in the Human Connectome Project-Early Psychosis (HCP-EP) sample(10).

In the frequency domain, the most relevant fMRI signal components are the slow oscillations between 0.01 and 0.1 Hz(11) with five canonical fMRI frequency bands, namely slow-5 (0.01 Hz-0.027 Hz), slow-4 (0.027-0.073 Hz), slow-3 (0.073-0.198 Hz), and slow-2 (0.198-0.5 Hz). Changes in these slow oscillations can reflect coordinated neural activity(12) via neurovascular coupling and hemodynamic response(13) due to local magnetic susceptibility changes(14). A slow-1 band overlaps with the lowest frequencies of the classic delta brainwave band but is beyond our Nyquist limit of 0.69 Hz. Slow-5 and slow-4, the slowest frequencies, have been associated with local field potential (LFP) periodicity(15) and with the hemodynamic response function(16). Slow-5 and slow-4 are widely associated with resting state networks properties, though some properties can be shown using slow-3 and slow-2 correlations(17). Slow-3 is partially filtered out to completely exclude slow-2, which includes respiratory artifacts at around 0.3 Hz(18). Studies that combine fMRI with electrophysiology(19) have shown that the strength of these slow BOLD fluctuations can track the envelope of the LFP power, especially in higher frequency γ-band(20,21).

Prior studies have found changes in power across specific resting-state frequency bands and reduced γ activity and signs of altered neurovascular coupling in schizophrenia(22). These findings suggest disruptions in the timing and coordination of neuronal activity, which are the primary features of interest in FC analysis, and have led to the identification of default mode network (DMN)(23), which is now acknowledged to play a role in both resting *and* task activity(24), and is central to many aspects of human cognition(23). Its disruption has been associated with schizophrenia(7). Importantly, lower frequency bands have been associated with reduced power in schizophrenia compared to controls for DMN regions(25).

Another widely studied system, the dorsal attention network (DAN), also known as the “top-down” attention network, which is altered in schizophrenia during attention-

requiring tasks(26), may be responsible for attentional deficits considered intrinsic to schizophrenia(27,28). The DAN supports distinct brain functions compared to the DMN, and the two networks are often anticorrelated(29,30). While the DMN may be involved in self-referential thinking, planning, retrospection, and prospection, the DAN is associated with hierarchical management of external stimuli and goal orientation. Altered interaction between the DMN and DAN may explain cognitive impairments and psychopathology in schizophrenia(31).

Examination of regional BOLD signal differences, often called first-order analyses(32,33), and brain network connectivity analyses, called second-order analysis(34), have led to a better understanding of psychosis, but they are limited when considering the systemic and inherently dynamic nature of brain activity(34,35). Using the HCP-EP fMRI cohort, we apply first-order, second-order, and the pairwise maximum entropy model (MEM), because the MEM simultaneously considers first- and second-order terms. The MEM, rooted in statistical physics, is a mathematical framework applicable to multivariate time-series data(36,37). It was initially used in cellular models of the retinal ganglion(38), hippocampal place cells(39), and primary visual cortex(40), and recently in the study of fMRI datasets(37,41-46). The model can be viewed as a generalization of the classic Ising model(47) into higher dimensional space that also includes a first-order term(48), expressing the likelihood of discrete states based on first- and second-order properties. Additionally, energy landscape analysis (ELA), which represents the global statistical structure of activation patterns over the length of fMRI acquisition, provides novel measures such as the basin structure and transitions through basin over time.

The MEM provides novel metrics that capture temporal dynamics better than other methods given the ambiguous nature for the fMRI signal(12). These include the 1) “energy” values that correlate negatively with probability of configuration of regional activation/deactivation patterns in a network (network states) (not metabolic energy); 2) the ELA (36), global structure of network configurations, including identifications local energy minima (basins or attractors)(49); and 3) basin transition rates over time and basin dwell times. Based on prior studies including ours(37,41-46), we hypothesized that MEM-derived features would provide novel nsights into the dynamic interactions within and between the DMN and DAN such as higher energy, basin transitions, and activation/deactivation switching. Additionally, few studies have examined DMN+DAN interaction at rest at the level of granularity of the HCP/Glasser atlas (50) in patients compared to controls.

Methods

Data and MRI Preprocessing

We examined T_1w anatomical MRI and the resting-state fMRI (anterior-to-posterior encoding) from the HCP-EP dataset(10). The HCP minimal preprocessing pipeline(51) using the Pittsburgh Supercomputing Center's (PSC) Bridges-2 system(52). T_1w images were processed using FreeSurfer 7.4.1(53) for intensity normalization, tissue labeling, and subcortical segmentation. Resting-state fMRI data were preprocessed using FSL 6.0, including rigid body motion correction, head motion estimation, and TOPUP(54,55).

The T_1w images were registered to EPI space, followed by aligning the atlas. The 360-node HCP/Glasser cortical atlas and 17 subcortical structures(50) were used, with subject-specific atlases created as previously described(56). We down-sampled T_1w images to the EPI images and applied nearest-neighbor interpolation to map subject-specific atlases to native EPI without warping the data. For each region (node), average voxel activation per timepoint was calculated to generate individual fMRI activation timeseries.

This study treats cortical regions as primary functional units(57) and uses the HCP/Glasser brain atlas rather than cluster or independent component analysis. In this atlas, the DMN and DAN are distinct: the DMN includes 34 bilateral nodes from the posterior cingulate, anterior cingulate, and lateral parietal areas(58), while the DAN comprises 24 bilateral nodes in the frontal, parietal, and occipital cortices (59) (**Supplemental Material S.1** for full list).

Psychopathology was assessed using the Positive and Negative Symptoms Scale (PANSS) and cognitive performance using auditory continuous performance test (ACPT) (d'), dimensional change card sort (DCCS), fluid cognition, executive function using Flanker test and list sorting working memory test (LSWMT).

First-order Analysis

For each subject and region, four fMRI frequency band powers were computed. Whole-brain patient and control data were compared using with MANCOVA, adjusting for age and sex. Next, group differences in each region were examined using between-subjects' effects correcting for multiple tests (**Supplemental Material S.1**). A separate MANCOVA model focused on slow-5 only for 58 DMN and DAN regions for group differences.

When nodal activity was coded as binary ("on" or "off"; see **Section 2.4**), each node's off-to-on and on-to-off transitions were counted over 410 fMRI timepoints per subject, defining the "number of microstate switches." This metric was compared to power in each frequency band at both the group and individual levels using population-wide and within-group correlations. ANOVA models assessed the link between band power and microstate switching. Finally, nodes were ranked by switch frequency, and group distributions for the top and bottom ten nodes were compared with the Kolmogorov–Smirnov test.

Second-order Analysis

Functional connectomes were derived from regionally averaged fMRI time-series by calculating Pearson's correlation coefficients (across time) for every pair of regions (network edges) (34). Analyses focused on the DMN, the DAN, and the combined 58-node DMN+DAN networks. Edges with a p-value less than 0.05 associated with the correlation strength between nodes were included where thresholding was applicable. The Brain Connectivity Toolbox (60) was employed to compute weighted network metrics, without applying threshold, nodal clustering coefficient (CC), modularity, strength, and efficiency. Nodal betweenness centrality (BC) was calculated on binary graphs.

Whole-graph and nodal network measures were compared between patients and controls using MANCOVA, controlling for age and sex including graph metrics for the 58-node DMN+DAN network as well as the 34-node DMN and 24-node DAN separately. Nodal-level analyses treated clustering, betweenness, and strength as repeated measures within subjects. Post-hoc between-subjects univariate ANCOVAs with multiple test corrections.

Edge-level functional connectivity was analyzed using all unique pairwise correlations, with significance at $\alpha=0.001$. These analyses were repeated for networks constructed within individual frequency bands, but the main results focus on full-spectrum functional connectivity. Analyses were performed for both individual frequency bands and full-spectrum networks, though the primary results emphasize full-spectrum connectivity. Frequency-specific FC networks and their graph measures across four bands are detailed in **Supplemental Material S.2**.

MEM Analysis

The pipeline from fMRI-to-MEM was previously published(46,49). The MEM energy function uses a vector h for first-order node activations and a matrix J for second-order pairwise activations. Parameters are derived from state vectors, where each entry is 1 for active nodes and –1 for inactive nodes.

The fMRI timeseries were z-scored(61) and a zero threshold was used to generate binary activity data for each node ("off" if ≤0, "on" if >0). Binary state probabilities were calculated by combining all subjects' data. Each subject's number of distinct binary states was measured for each node group, and distributions were compared between groups with the two-sample KS test. Maximum-likelihood estimation was then applied to estimate MEM parameters (*h* and *J*) using average node activity and pairwise correlations at the group level.

This procedure was repeated for 6 collections of nodes: the most (top) and least (bottom) frequently state-switching DMN, DAN, and DMN+DAN nodes. After model fitting, each participant's fMRI binary state time series (410 timepoints) was converted into an MEM-based energy timeseries, representing their energy trajectory. The sum of these energies forms the non-time-resolved "energy trace." Energy trace distributions for patients and controls were compared across the six systems using two-sample KS tests.

After estimating MEM parameters, dysconnectivity graphs of local energy minima were constructed using binary Hamming distances(49), where neighboring states differ by a single microstate switch. Each local minimum defines a bsin, and non-minimal states are assigned to basins if their shortest neighbo-to-neighbor path to the minimum decreases in energy. While these paths represent conceptual trajectories, real fMRI time-series often show energy increases between consecutive states, allowing transitions across multiple basins. Basin transition rates and dwell times per subject were calculated and compared across groups with two-sample KS-tests for each system. MEM analyses used a modified *elapy* package (https://github.com/okumakito/elapy/tree/main/elapy) and custom MATLAB code.

Association with cognition

We used t-tests and ANOVA to assess age and sex distribution differences. MANCOVA examined group effects on first- and second-order MEM metrics and cognitive measures, adjusting for age and sex. We then tested correlations between imaging-derived variables that differed by group and PANSS scores, attention (*d'* from ACPT), LSWMT scores, Flanker, and DCCS scores from the NIH Toolbox using partial correlations controlling for age, sex, and diagnosis, correcting for multiple testing, with additional analyses by group.

Results

Sample Characteristics

Our final sample consisted of 165 subjects (109 patients and 56 controls) after excluding nine for either not having a complete cortical parcellation, failing preprocessing, or not having required number of timepoints; other studies included 93 to 124 patients(62-

64). Patients were younger than controls (t=3.33, p=0.001) with no sex distribution differences (χ^2=0.21, p=0.64). Most patients had non-affective psychosis **(Table 1)**.

Group	N	Mean Age (years)	SD Age (years)	Females	Males	Affective	Non-Aff
Controls	56	24.9	4.0	19 (34%)	37 (66%)	0	0
Patients	109	22.8	3.8	41 (38%)	68 (62%)	26	83
Schizophrenia	58	24.93	4.00	19	39		
Schizoaffective d/o	14	22.17	3.40	4	10		
Schizophreniform d/o	6	24.71	4.28	2	4		
Delusional d/o	1	23.17		1	0		
Brief psychotic d/o	1	30.75		1	0		
Psychosis NOS	3	23.41	5.33	0	3		
Major depressive d/o	20	21.50		12	8		
Bipolar disorder	22	24.14	4.30	8	14		

Table 1. Clinical and demographic data (some participants may have more than one diagnosis as these are lifetimes rates)

First-Order Results

At the whole-brain level, there were significant differences in regional power in all frequency bands, with patients always exhibiting lower power (**Supplemental Material S.1**).

A MANCOVA analysis of 377 regions across 4 frequency bands revealed significant group differences (Wilk's λ=0.01, F=354.14, p=0.04). After Bonferroni correction, 215 regions had lower **frequency band power in p**atients than controls. In the DMN and DAN networks, 13 out of 58 regions showed notably reduced BOLD frequency power (**Supplemental Material S.1**). Affected DMN Glasser parcellations (sections) included left TPOJ3 (temporo-parieto-occipital junction 3) and IP1 (inferior parietal), and right POS1 and POS2 (posterior cingulate); DAN parcellations (sections) included bilateral MST and MT (parieto-temporal cortex), 7PC, bilateral VIP, and right 7am (superior parietal), and right PH (MT+Complex).

We observed a significant negative correlation between microstate switching and band power across all frequency bands. This correlation was weaker in faster bands (slow-3 and slow-2, often linked to respiratory artifacts) but stronger in slower bands (slow-5, slow-4), both at the group and individual levels **(Figure 1A, 1B)**. In both whole-population and within-group ANOVA tests (**Supplemental Material S.1**), all post-hoc F-tests for band-wise differences in switching-to-power correlation were significant (p<0.001).

Among the top ten most frequently switching and bottom ten least frequently switching nodes for both DMN and DAN (40 unique nodes), 21 showed significant group differences in microstate switching frequency **(Figure 1C).** Patients exhibited higher group-

averaged microstate switching, with no difference seen in the least frequently switching DMN nodes. Of 13 regions with different band power, 9 also differed in microstate switching.

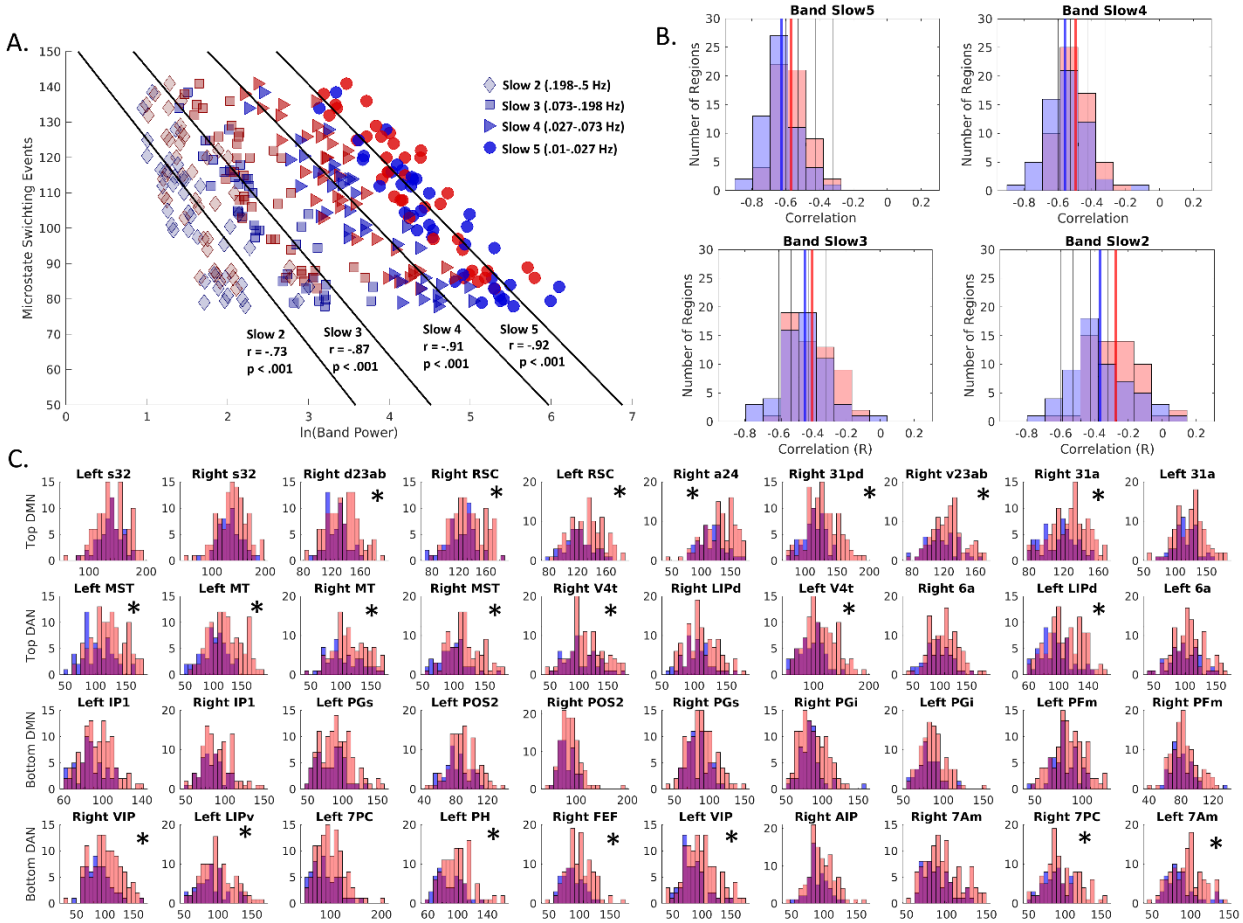

Figure 1. First Order Results. A) Correlations between power in frequency bands and counts of microstate switching events, where each scatter point represents the group-level average (controls in blue, patients in red) for a region. **B)** Groupwise population histograms for individual correlations: Distributions across subjects of correlations between switching and power, for each band, by group. Black vertical lines show band averages from all bands (including sibling subplots), whereas blue and red vertical lines show control and patient (respectively) group level average correlations (of regions) for that subplot. Histograms show nodal distributions of correlations calculated across subjects within a group. **C)** Microstate switching by group: asterisks indicate significant differences in patient-control distributions by KS-test after FDR correction at level alpha = 0.05. For both DMN and DAN, the top (most microstate switching events) and bottom (least microstate switching events) 10 regions are shown. Histograms represent all individuals, where y-axis is number of participants and x-axis is number of microstate switching events in the given region over the course of the resting state fMRI acquisition.

Second Order Results

At the whole-graph level, a significant group effect was observed across average clustering, global efficiency, modularity, and average betweenness centrality (MANCOVA; Wilks' λ=0.94, F(3,159)=3.15, p=0.020). Post-hoc between-subjects' effects with Bonferroni correction showed all measures differed between groups (all p<0.015); patients had lower average clustering and efficiency but higher modularity and betweenness centrality than controls.

Analyses of frequency-specific networks yielded similar results, though fewer differences were found in slow-2 bands (**Supplemental Material S.2**). Therefore, subsequent analyses focused on full-spectrum connectivity. At the nodal level, MANCOVA controlling for age and sex found no overall group effect, on the combined nodal network measures (clustering, betweenness, and strength; Wilks' λ=0.99, F(2,160)=0.05, p=0.95), but Bonferroni-corrected univariate between-subjects' tests indicated that patients had higher betweenness centrality (p=0.011) and lower clustering coefficient (p=0.015) and strength (p=0.008), suggesting opposing effects masked significance in multivariate testing.

		DMN		DAN		DMN+DAN	
Metric	**Group**	**Mean**	**SD**	**Mean**	**SD**	**Mean**	**SD**
Clustering	Controls	**0.41	0.09	**0.49	0.14	**0.36	0.11
	Patients	**0.36	0.11	**0.43	0.13	**0.30	0.11
Modularity	Controls	**0.07	0.03	0.06	0.04	**0.12	0.05
	Patients	**0.09	0.03	0.07	0.04	**0.15	0.06
Efficiency	Controls	**0.47	0.08	**0.53	0.11	**0.43	0.09
	Patients	**0.42	0.09	**0.48	0.11	**0.39	0.09
Betweenness	Controls	23.37	11.12	12.02	9.36	**54.35	27.54
	Patients	26.61	12.57	14.03	7.80	**67.59	28.94

Table 2. Graph metrics for second-order comparisons. Network connectivity metrics for the entire 58-node DMN+DAN network, as well as the 34-node DMN and 24-node DAN shown separately. Asterisks indicate significance at **p<0.01.

Differences between groups at the individual-edge level are visually noticeable (**Figures 2A, 2B).** Among 1,653 edges in this 58-node network, 181 (about 10%) showed significant group differences (KS-tests, α=0.001), with patients exhibiting more negatively weighted edges (**Supplemental Material S.2**) indicating weaker connections, reduced clustering, and increased modularity in psychosis patients at the node and graph levels.

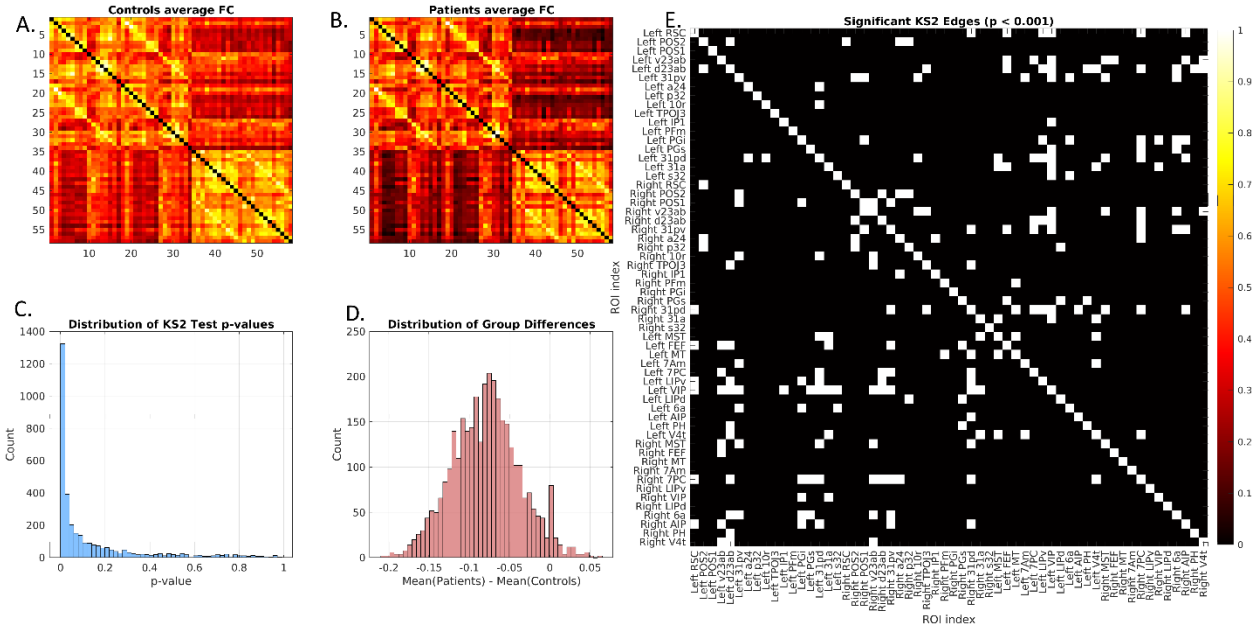

Figure 2. Second Order Results. A) The control-group average FC for edges between all DMN and DAN nodes. **B)** The patient-group average FC for all unique DMN and DAN node-pairs. **C)** Histogram of p-values for two-sample KS-test of FC edge weight difference by group over all tests. **D)** Histogram of difference in group level average edge weight. **E)** The binary outcome of null hypothesis rejection at level alpha 0.001 for the two-sample KS-test by edge.

MEM Results

MEMs were applied to concatenated binary activation data from six systems, each with ten nodes. Analyses included the highest and lowest switching DMN, DAN, and combined DMN+DAN systems (with five nodes each from DMN and DAN). All models fit successfully (**Supplemental Material S.3**).

Patients consistently showed a greater number of distinct node states than controls across all six systems, regardless of sample size (**Figure 3**). Significant differences were found in the distributions for top DMN (*KS*=0.32, *p*<0.001), bottom DMN (*KS*=0.31, *p*=0.001), top DAN (*KS*=0.30, *p*=0.002), bottom DAN (*KS*=0.30, *p*=0.003), top DMN+DAN (*KS*=0.37, *p*<0.001), and bottom DMN+DAN (*KS*=0.30, *p*=0.001) with patients consistently exhibiting more unique states than the controls in each system.

A permutation test comparing distinct states across 500 random node sets showed that, in the DMN, DAN, and DMN+DAN systems, patients had more distinct states than controls in over 95% of permutations (**Supplemental Material S.3**). There were no differences between non-affective and affective psychosis patients, but both differed from controls (**Supplemental Material S.4**).

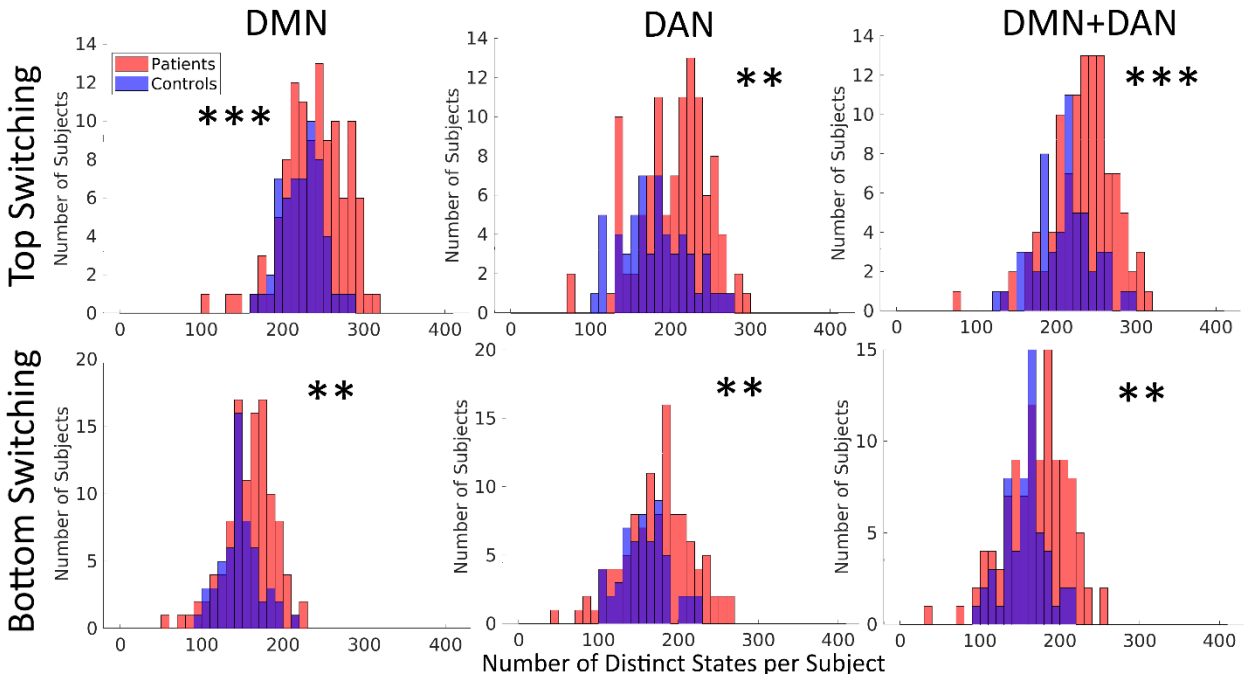

Figure 3. The number of distinct states per subject is shown in two histograms (one per group) for the six systems. Asterisks indicate significance level of difference of distribution by two-sample KS-test, where: **p <0.01; ***p <0.001.

A MANCOVA model controlling for age and sex that included all MEM metrics (top and bottom distinct states, energy trace, basin transitions in the DMN, DAN, and DMN+DAN) was significant for patient-control differences (Wilk's λ=0.82, F=1.79, p=0.03). Posthoc between-subjects' effects showed all metrics were higher among patients than controls (p<0.03), but bottom energy trace in all three systems were not different after Bonferroni corrections. Similar trends appeared when comparing non-affective psychosis, affective psychosis, and controls, with most differences seen between non-af**fective psychosis and controls;** top energy trace was highest in non-affective psychosis, intermediate in affective psychosis, and lowest in controls (**Supplemental Material S.3 and 4**).

After fitting MEMs at the whole-sample level, we computed state energies, which is inversely related to state probability, and mapped each subject's binary fMRI time course to energy time series showing significant patient–control differences for top switching systems only: DMN top (KS=0.29, p=0.003) DAN top (KS=0.34, p<0.001) and DMN+DAN top (KS=0.33, p<0.001) (**Figure 4)**. This pattern mirrors first-order results, where group differences were present in top-switching DMN nodes only. For second-order metrics, the DAN showed the highest similarity between groups.

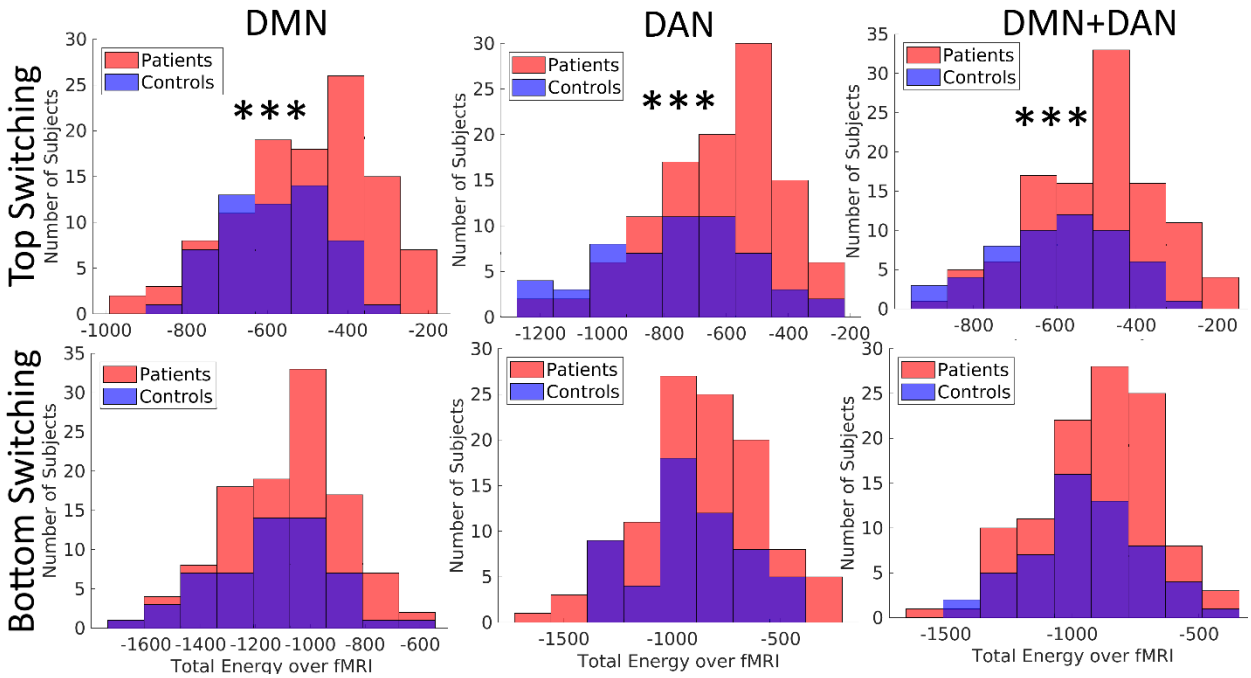

Figure 4. Histograms of energy traces for individuals in each group and each network, defined by the total energy values across all observed states per subject. The figure shows that the patients have higher traces than controls in the top switching systems. Two-sample KS-test: **p<0.01; ***p<0.001.

A single MEM was fit to combined patient and control data for each network, providing a shared energy landscape for state trajectory comparison (**Figure 5**). Basin structure varied: the bottom-switching DMN had a complex landscape, while the top-switching DMN centered on all-on and all-off states; this pattern was reversed but less pronounced in the DAN. For all six systems, all-on and all-off basins were dominant. The combined DMN+DAN networks also revealed basins for DMN-only and DAN-only activation, indicating dynamic shifts among co-activation, co-deactivation, and mutually exclusive states, likely due to their anti-correlational relationship (**Figure 2**).

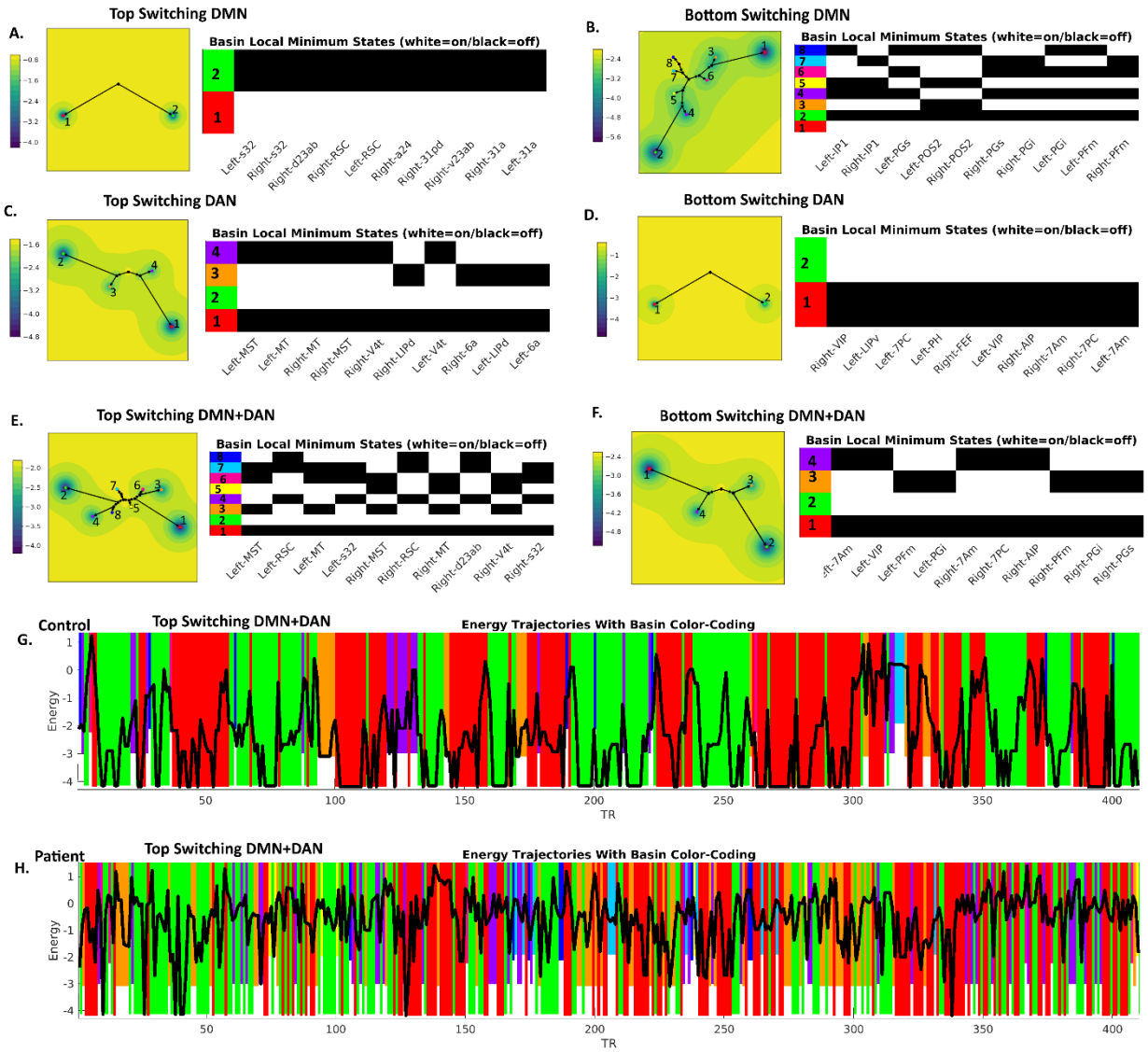

Figure 5. Energy minima and basin switching within energy landscapes. A. Energy landscapes including minima and associated basins (left) and activation state configurations for minima (right) for top switching DMN. Analogous plots are shown for: **B.** Bottom switching DMN, **C.** Top switching DAN, **D.** Bottom switching DAN, **E.** Top switching DMN+DAN, **F.** Bottom switching DMN+DAN. **G**. The color-coded (by basin) energy trajectory for the 410 fMRI timepoints in an example control subject. **H.** The color-coded (by basin) energy trajectory for the 410 fMRI timepoints in an example patient. Both **G** and **H** use the basin color coding given in **E** and present results from an example participant's top switching DMN+DAN. Thick black line represents energy value; each colored rectangle represents occupation of a corresponding basin; downwards extent of rectangles represent basin depth. Note that the specific state associated with each color does not agree across systems, but colors are assigned in the same order for all systems (e.g., red always identifies the system's lowest energy basin, followed by green, and so on).

Basin transition counts differed between groups (**Figure 6**), with significant differences for top-switching DMN, DAN, DMN+DAN, and bottom-switching DMN+DAN (all KS>0.30, p≤0.002). Patients showed more total state transitions, but specific basin transition rates were similar to controls **(Supplemental Material S.**5), indicating increased transition frequency without altered temporal patterns. Direct transitions between DMN-only and DAN-only states were rare (<5%), while remaining in exclusive basins (~40%) or switching from all-nodes-on to all-nodes-off basins (~15%) was more common. In DMN+DAN networks, lowest-energy basins corresponded to DMN-only or DAN-only activation (basins 3 and 4 in **Figure 5E,F**) and direct switches between these were minimal (2-4%, **Supplemental Material S.5**), implying largely independent switching during rest. There were no significant differences in basin transitions between non-affective and affective psychosis versus controls, though non-affective patients differed from controls across all systems **(Supplemental Material S.4)**.

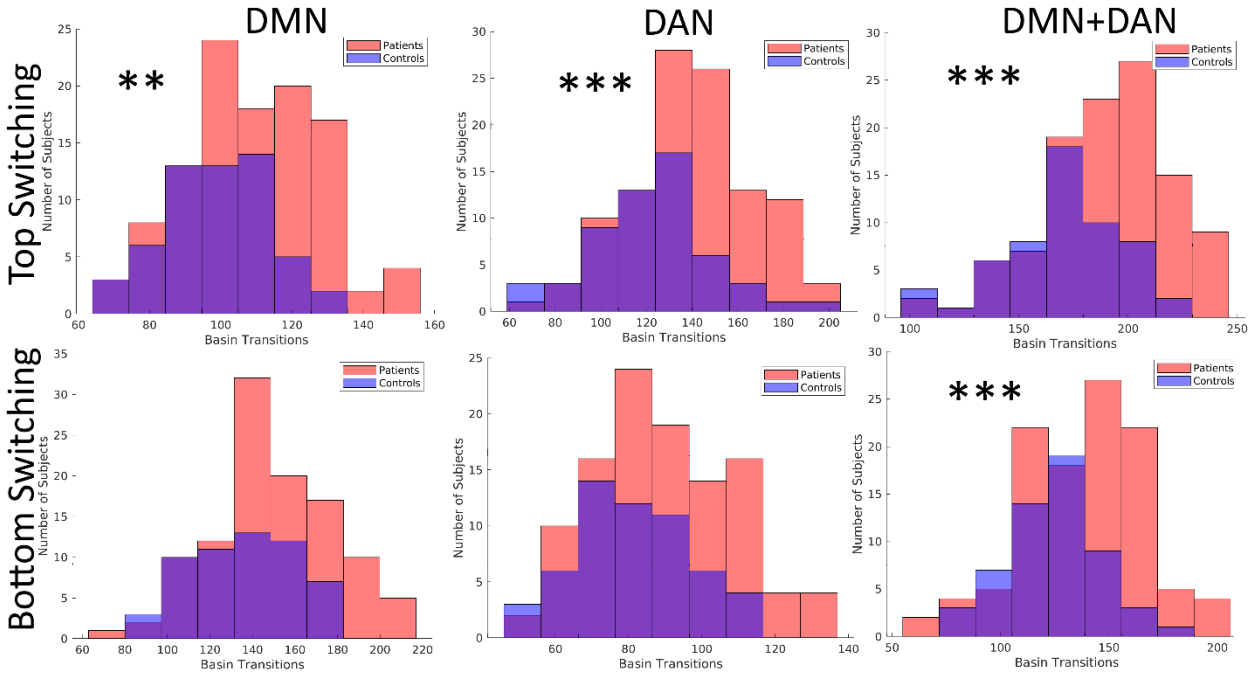

Figure 6. Numbers of basin transitions per subject by system and group. Top row indicates top microstate switching networks, bottom row indicates bottom microstate switching networks. From left to right: DMN, DAN, DMN+DAN. Asterisks indicate significance level of difference of distribution by two-sample KS-test: **p <0.01; ***p <0.001.

Average dwell time per participant was calculated for each basin and compared between groups (**Figure 7**). Some basins had significantly shorter dwell times in patients, while others did not differ. In the top-switching DMN+DAN system, patients spent less time

in basin 1 (all-off) and basin 3 (DMN-only). For the bottom-switching DMN+DAN, patients also had reduced dwell times in basin 2 (all-on) and basin 3 (DAN-only).

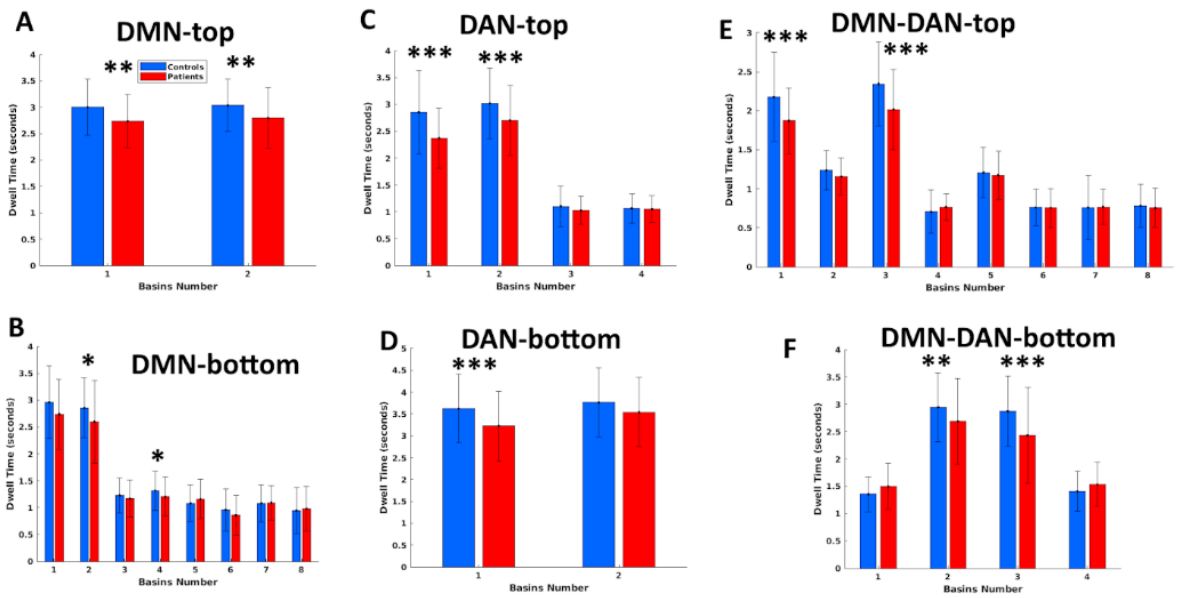

Dwell Times	Basin 1	Basin 2	Basin 3	Basin 4	Basin 5	Basin 6	Basin 7	Basin 8
DMN-t	.29**	.29**						
DMN-b	.19	.24*	.19	.25*	.21	.08	.14	.10
DAN-t	.34***	.27**	.13	.10				
DAN-b	.34***	.19						
DMN-DAN-t	.31***	.20	.34***	.08	.11	.09	.09	.14
DMN-DAN-b	.17	.30**	.39***	.14				

Figure 7. Basin dwell times often differ between groups. **A-F.** Average dwell times for basins associated with all energy minima for controls (blue) and patients (red) for indicated networks. Table shows KS-statistics; asterisks there and above indicate significance of KS-test: *p <0.05, **p <0.01, ***p <0.001. In every case where significance was detected, the patients always had a lower average dwell time for the basin. A variable number of basins was detected per system; where cells are grey (blank), the system did not have that many basins.

Associations with cognitive and psychopathology measures

Cognitive performance: MANCOVA analysis of cognitive scores, adjusted for diagnosis, age, and sex, was significant (Wilk's λ=0.66, $F(14,280)=4.60$, $p<0.001$). All test scores except fluid cognition differed significantly (all $p<0.001$). Games-Howell corrected posthoc tests revealed that, aside from fluid intelligence, controls and non-affective psychosis patients differed on all measures, but affective psychosis patients did not. Only DCCS scores distinguished affective from non-affective psychosis groups.

First-order metrics: Controlling for diagnostic status, age, and sex, band power 5 in left IP1 (r=0.31), left PH (r=0.33), and right POS2 (r=0.27) was positively correlated with working memory (all p<0.001, FDR-corrected). Posthoc tests showed significant

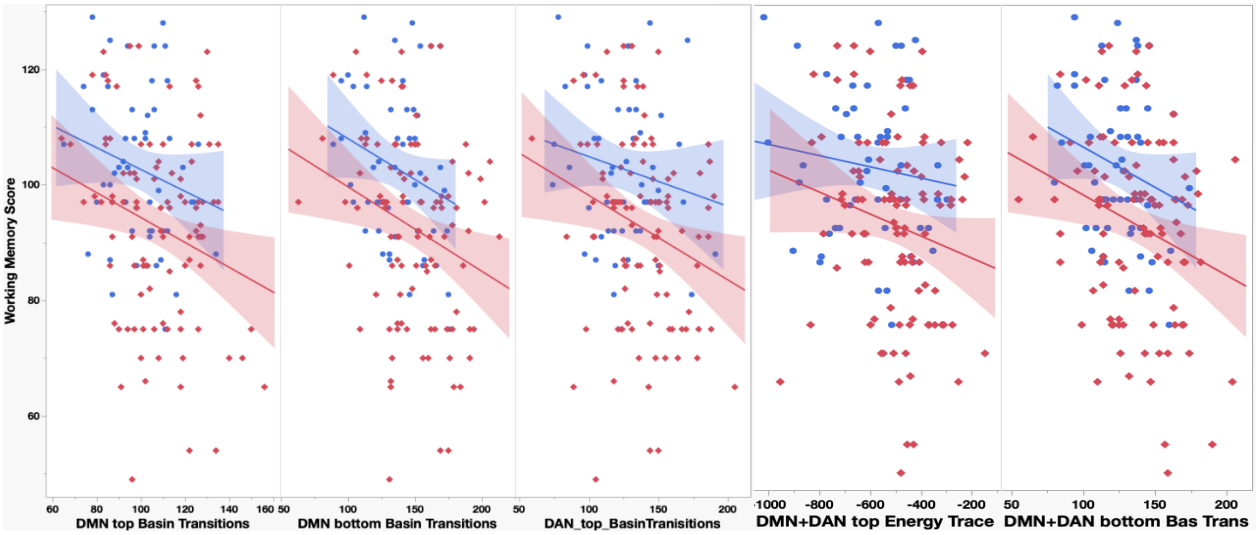

Figure 8: Correlation of working memory with MEM metrics. Red diamonds and fit line represent scores for early psychosis patients and blue dots with blue fit line represent healthy controls. Partial correlation controlling for age, sex, and diagnostic status was first conducted followed by correlations for each group. All correlations for the entire sample of patients and controls were significant after correcting for multiple tests using Bonferroni approach. Groupwise correlations showed that negative correlations retained significance after multiple test corrections with all MEM metrics, but healthy controls showed significant correlations with DMN top and bottom basin transitions and DMN+DAN bottom basin transitions but not with DAN top basin transitions and DMN+DAN top energy trace.

correlations among both patients and controls. The first-order metrics did not correlate with psychopathology severity.

Second-order metrics: None of the FC graph metrics correlated with cognitive performance or psychopathology severity.

MEM-derived metrics: After controlling for age, sex, and diagnosis, several MEM-derived measures (DMN top/bottom basin transitions, DAN top basin transitions, DMN+DAN energy trace) showed significant negative correlations with working memory after false discovery rate corrections (partial r from –0.21 to –0.27, all p<0.004). No MEM-derived metric related to total PANSS score, but DAN and DMN+DAN energy trace were positively correlated with positive symptom scores after multiple test correction (critical α>0.001) (**Figure 8**).

Discussion

We contrasted first-order, second-order, and MEM models in a multiversal analysis in early psychosis and controls. Patients showed reduced BOLD signal frequency band

powers, especially in band 5, in multiple regions supporting prior studies(25) and increased binary state switching in DMN and DAN nodes (except bottom-switching DMN regions) compared to controls (**Figure 1C**) these changes were largely explained by non-noise band power differences **(Figure 1A)**, consistent with larger amplitude, wider envelope deflections drive microstate transitions. Our findings support previous amplitude of low frequency fluctuations (ALFF) studies(32,65,66) and show that reduced band power is linked to higher microstate switching. Our extension of band power frequency examination to binary state switching at finer temporal scales adds a new dimension to the results providing preliminary mechanistic insight into dynamic changes in BOLD signals related to clinical groups. However, only a few regions correlated with cognitive performance but none with psychopathology suggesting the limited clinical significance of first-order analyses.

Psychosis was associated with more anti-correlated DMN+DAN edges, weaker connections, lower clustering and efficiency, and higher modularity and betweenness centrality (**Table 2; Figure 2; Supplemental Material 1.2**) supporting prior research(7). These findings suggest greater segregation with weaker local cohesion in patients, which is most evident in DMN+DAN, and less when either network studied alone. Lack of correlation with cognition and psychopathology may be due to the high individual variability of connectivity strength in these regions(67) and raises questions about the clinical relevance of relying entirely on FC metrics.

In the MEM analysis, patients exhibited more distinct binary states per system (**Figure 3**) with significantly higher group-level energy traces than controls, an effect not observed in bottom switching systems (**Figure 4**). These findings demonstrate that psychosis is associated with increased higher-energy (lower-probability) brain states and switch more often with reduced dwell time suggesting instability of resting networks compared to controls. Basin transitions were triggered when energy peaked at certain points, hinting that criticality may drive these transitions; future studies should formally assess this possibility. Controls showed lower energy traces, fewer basin transitions and longer dwell times indicating greater network stability (**Figure 5 and 6**). Differences were mainly observed in non-affective psychosis versus controls, while comparisons involving affective psychosis were limited by small sample size **(Supplemental Material S.**4). These findings extend our earlier finding among adolescent-onset schizophrenia, and schizophrenia, bipolar disorder, and major depression(46,68) proposing a mechanism for unstable networks. Non-significant differences in basin transition patterns (**Figure 7; Supplemental Material 1.5**), suggest faster switching among higher-energy states without altering transition architecture. These results were confirmed across 500 permutations for each system confirming they are not due to random node selection (**Supplemental Material 1.3**).

We observed positive correlation of BOLD signals with working memory in 3 of 58 regions, but not with psychopathology severity. Second-order FC graph metrics showed no association with cognitive or psychopathology measures. In contrast, multiple MEM metrics, especially basin transitions and energy trace per subject in all three systems, were positively correlated with working memory performance and psychopathology severity. Higher basin transitions and energy suggest functional network instability supporting our previous findings linking energy to executive function in adolescent-onset schizophrenia(46). Correlations were specific to working memory, suggesting MEM metrics from resting fMRI may be more specific to working memory than others like fluid intelligence or attention; task fMRI might be more preferable for such examination. Lack of correlation with executive function may reflect differences in tasks across studies: Flanker task in this data and Penn Conditional Exclusion Test in prior study(46). Notably, DAN and DAN+DMN basin transitions and energy trace correlated with positive symptoms but not negative and general psychopathology symptoms. These findings are partly consistent with positive correlation of energy with total psychopathology among adolescent-onset schizophrenia(46). Further investigations are needed to elucidate the mechanisms related to such correlations.

First-order results often rely on higher/lower BOLD intensity averaged over the entire acquisition, but interpretations vary and lack time resolution(4,69). Common second-order methods like static FC are also not time resolved because the correlations are parameterized over time. MEM offers a key advantage by capturing system interactions consistent with neuroscience principles and preserving both first- and second-order features, while addressing interdependence and temporal nonlinearity of pairwise correlations unlike FC analysis which treats correlations as independent(70), while providing temporal resolution and unique metrics. However, MEM's limitation is model size, constrained by exponential growth in states and parameters with more nodes, though this can be partially mitigated through alternative designs(37).

The DMN and DAN are evolutionarily conserved resting network(71) that are extensively studied(72,73) using MRI and EEG in humans(42) and animals(74). Their interactions may support top-down attention by balancing internal and external thoughts (75); both influence which stimuli are attended to. This interplay could explain delusional thinking(76) and/or disorganization of thought(77). Integrating multiversal analysis with established brain network methods, such as MEM, may clarify spatial and temporal changes in brain activity linked to cognitive deficits.

Acknowledgements

This work was funded by the US National Institute of Mental Health (NIMH) through R01MH112584, R01MH115026, and R01MH137090 (KMP).

We thank the Pittsburgh Supercomputing Center for providing computational resources through ACCESS Discover grant BIO200047.

Nicholas Theis managed the data, conducted the analyses, and drafted the early versions and edited the manuscript; **Bowei Ouyang** helped in the MEM analyses in particular and edited the manuscript; **Ella O'Rourke** conducted the analysis of first-order data and edited the results tables; **Jonathan Rubin** and **Jyotika Bahuguna** refined the conceptual basis, oversaw mathematical models, edited the manuscript, and interpreted the results; **Joshua Cape** and **Satish Iyengar** oversaw the statistical analyses and edited the manuscript; **Konasale Prasad** obtained the funds, oversaw the data management, conceived the idea and participated in discussions to refine the idea, oversaw the entire analyses, and edited and finalized the manuscript.

Disclosures

The authors have nothing to disclose that is relevant for this manuscript.

References

1. O'Neill A, Mechelli A, Bhattacharyya S (2019): Dysconnectivity of Large-Scale Functional Networks in Early Psychosis: A Meta-analysis. *Schizophrenia bulletin*. 45:579–590.
2. Keshavan MS, Eack SM, Prasad KM, Haller CS, Cho RY (2017): Longitudinal functional brain imaging study in early course schizophrenia before and after cognitive enhancement therapy. *NeuroImage*. 151:55–64.
3. Stolz E, Pancholi KM, Goradia DD, Paul S, Keshavan MS, Nimgaonkar VL, et al. (2012): Brain activation patterns during visual episodic memory processing among first-degree relatives of schizophrenia subjects. *NeuroImage*. 63:1154–1161.
4. Glahn DC, Ragland JD, Abramoff A, Barrett J, Laird AR, Bearden CE, et al. (2005): Beyond hypofrontality: a quantitative meta-analysis of functional neuroimaging studies of working memory in schizophrenia. *Human brain mapping*. 25:60–69.
5. Ragland JD, Laird AR, Ranganath C, Blumenfeld RS, Gonzales SM, Glahn DC (2009): Prefrontal activation deficits during episodic memory in schizophrenia. *The American journal of psychiatry*. 166:863–874.
6. Cai M, Wang R, Liu M, Du X, Xue K, Ji Y, et al. (2022): Disrupted local functional connectivity in schizophrenia: An updated and extended meta-analysis. *Schizophrenia*. 8:93.
7. Voineskos AN, Hawco C, Neufeld NH, Turner JA, Ameis SH, Anticevic A, et al. (2024): Functional magnetic resonance imaging in schizophrenia: current evidence, methodological advances, limitations and future directions. *World Psychiatry*. 23:26–51.
8. Steegen S, Tuerlinckx F, Gelman A, Vanpaemel W (2016): Increasing Transparency Through a Multiverse Analysis. *Perspect Psychol Sci*. 11:702–712.
9. Dafflon J, F. Da Costa P, Váša F, Monti RP, Bzdok D, Hellyer PJ, et al. (2022): A guided multiverse study of neuroimaging analyses. *Nature Communications*. 13:3758.
10. Jacobs GR, Coleman MJ, Lewandowski KE, Pasternak O, Cetin-Karayumak S, Mesholam-Gately RI, et al. (2025): An Introduction to the Human Connectome Project for Early Psychosis. *Schizophrenia bulletin*. 51:658–671.
11. Zuo XN, Di Martino A, Kelly C, Shehzad ZE, Gee DG, Klein DF, et al. (2010): The oscillating brain: complex and reliable. *NeuroImage*. 49:1432–1445.
12. Epp SM, Castrillón G, Yuan B, Andrews-Hanna J, Preibisch C, Riedl V (2025): BOLD signal changes can oppose oxygen metabolism across the human cortex. *Nature neuroscience*.
13. Kennerley AJ, Harris S, Bruyns-Haylett M, Boorman L, Zheng Y, Jones M, et al. (2012): Early and late stimulus-evoked cortical hemodynamic responses provide insight into the neurogenic nature of neurovascular coupling. *Journal of cerebral blood flow and metabolism : official journal of the International Society of Cerebral Blood Flow and Metabolism*. 32:468–480.
14. Drew PJ (2019): Vascular and neural basis of the BOLD signal. *Curr Opin Neurobiol*. 58:61–69.

15. Penttonen M, Buzsáki G (2003): Natural logarithmic relationship between brain oscillators. *Thalamus & Related Systems*. 2:145–152.
16. Logothetis NK (2003): The Underpinnings of the BOLD Functional Magnetic Resonance Imaging Signal. *The Journal of Neuroscience*. 23:3963.
17. Gohel SR, Biswal BB (2015): Functional integration between brain regions at rest occurs in multiple-frequency bands. *Brain Connect*. 5:23–34.
18. Birn RM, Diamond JB, Smith MA, Bandettini PA (2006): Separating respiratory-variation-related fluctuations from neuronal-activity-related fluctuations in fMRI. *NeuroImage*. 31:1536–1548.
19. Moon HS, Jiang H, Vo TT, Jung WB, Vazquez AL, Kim SG (2021): Contribution of Excitatory and Inhibitory Neuronal Activity to BOLD fMRI. *Cereb Cortex*. 31:4053–4067.
20. Logothetis NK, Pauls J, Augath M, Trinath T, Oeltermann A (2001): Neurophysiological investigation of the basis of the fMRI signal. *Nature*. 412:150–157.
21. Magri C, Schridde U, Murayama Y, Panzeri S, Logothetis NK (2012): The Amplitude and Timing of the BOLD Signal Reflects the Relationship between Local Field Potential Power at Different Frequencies. *The Journal of Neuroscience*. 32:1395.
22. Hirano Y, Oribe N, Kanba S, Onitsuka T, Nestor PG, Spencer KM (2015): Spontaneous Gamma Activity in Schizophrenia. *JAMA psychiatry*. 72:813–821.
23. Menon V (2023): 20 years of the default mode network: A review and synthesis. *Neuron*. 111:2469–2487.
24. Finn ES (2021): Is it time to put rest to rest? *Trends in cognitive sciences*. 25:1021–1032.
25. Garrity AG, Pearlson GD, McKiernan K, Lloyd D, Kiehl KA, Calhoun VD (2007): Aberrant "default mode" functional connectivity in schizophrenia. *The American journal of psychiatry*. 164:450–457.
26. Keane BP, Krekelberg B, Mill RD, Silverstein SM, Thompson JL, Serody MR, et al. (2023): Dorsal attention network activity during perceptual organization is distinct in schizophrenia and predictive of cognitive disorganization. *The European journal of neuroscience*. 57:458–478.
27. Bleuler E (1911): Dementia praecox or the group of schizophrenias.
28. Luck SJ, Gold JM (2008): The construct of attention in schizophrenia. *Biological psychiatry*. 64:34–39.
29. Esposito R, Cieri F, Chiacchiaretta P, Cera N, Lauriola M, Di Giannantonio M, et al. (2018): Modifications in resting state functional anticorrelation between default mode network and dorsal attention network: comparison among young adults, healthy elders and mild cognitive impairment patients. *Brain imaging and behavior*. 12:127–141.
30. Owens MM, Yuan D, Hahn S, Albaugh M, Allgaier N, Chaarani B, et al. (2020): Investigation of Psychiatric and Neuropsychological Correlates of Default Mode Network and Dorsal Attention Network Anticorrelation in Children. *Cereb Cortex*. 30:6083–6096.
31. Martin AK, Mowry B, Reutens D, Robinson GA (2015): Executive functioning in schizophrenia: Unique and shared variance with measures of fluid intelligence. *Brain Cogn*. 99:57–67.

32. Hoptman MJ, Zuo XN, Butler PD, Javitt DC, D'Angelo D, Mauro CJ, et al. (2010): Amplitude of low-frequency oscillations in schizophrenia: a resting state fMRI study. *Schizophrenia research*. 117:13–20.
33. Amaro E, Jr., Barker GJ (2006): Study design in fMRI: basic principles. *Brain Cogn*. 60:220–232.
34. Mohanty R, Sethares WA, Nair VA, Prabhakaran V (2020): Rethinking Measures of Functional Connectivity via Feature Extraction. *Scientific Reports*. 10:1298.
35. Reid AT, Headley DB, Mill RD, Sanchez-Romero R, Uddin LQ, Marinazzo D, et al. (2019): Advancing functional connectivity research from association to causation. *Nature neuroscience*. 22:1751–1760.
36. Masuda N, Islam S, Thu Aung S, Watanabe T (2025): Energy landscape analysis based on the Ising model: Tutorial review. *PLOS Complex Systems*. 2:e0000039.
37. Prasad K, Bowei O, Theis N (2025): From microstates to macroscales: A Critical Review of Maximum Entropy Modeling and Energy Landscape Analysis in functional MRI. *Res Sq*.
38. Simoncelli EP, Olshausen BA (2001): Natural image statistics and neural representation. *Annu Rev Neurosci*. 24:1193–1216.
39. Fuhs MC, Touretzky DS (2006): A spin glass model of path integration in rat medial entorhinal cortex. *The Journal of neuroscience : the official journal of the Society for Neuroscience*. 26:4266–4276.
40. Tang A, Jackson D, Hobbs J, Chen W, Smith JL, Patel H, et al. (2008): A maximum entropy model applied to spatial and temporal correlations from cortical networks in vitro. *The Journal of neuroscience : the official journal of the Society for Neuroscience*. 28:505–518.
41. Watanabe T, Hirose S, Wada H, Imai Y, Machida T, Shirouzu I, et al. (2013): A pairwise maximum entropy model accurately describes resting-state human brain networks. *Nat Commun*. 4:1370.
42. Das A, de Los Angeles C, Menon V (2022): Electrophysiological foundations of the human default-mode network revealed by intracranial-EEG recordings during resting-state and cognition. *NeuroImage*. 250:118927.
43. Ezaki T, Watanabe T, Ohzeki M, Masuda N (2017): Energy landscape analysis of neuroimaging data. *Philos Trans A Math Phys Eng Sci*. 375:20160287.
44. Gu S, Cieslak M, Baird B, Muldoon SF, Grafton ST, Pasqualetti F, et al. (2018): The Energy Landscape of Neurophysiological Activity Implicit in Brain Network Structure. *Sci Rep*. 8:2507.
45. Kang J, Jeong SO, Pae C, Park HJ (2021): Bayesian estimation of maximum entropy model for individualized energy landscape analysis of brain state dynamics. *Human brain mapping*. 42:3411–3428.
46. Theis N, Bahuguna J, Rubin JE, Banerjee SS, Muldoon B, Prasad KM (2025): Energy of Functional Brain States Correlates With Cognition in Adolescent-Onset Schizophrenia and Healthy Persons. *Human brain mapping*. 46:e70129.
47. Amit DJ, Gutfreund H, Sompolinsky H (1985): Spin-glass models of neural networks. *Phys Rev A Gen Phys*. 32:1007–1018.

48. Yeh F-C, Tang A, Hobbs JP, Hottowy P, Dabrowski W, Sher A, et al. (2010): Maximum Entropy Approaches to Living Neural Networks. *Entropy*. 12:89–106.
49. Ishida T, Yamada S, Yasuda K, Uenishi S, Tamaki A, Tabata M, et al. (2024): Aberrant brain dynamics of large-scale functional networks across schizophrenia and mood disorder. *NeuroImage: Clinical*. 41:103574.
50. Glasser MF, Coalson TS, Robinson EC, Hacker CD, Harwell J, Yacoub E, et al. (2016): A multi-modal parcellation of human cerebral cortex. *Nature*. 536:171–178.
51. Glasser MF, Sotiropoulos SN, Wilson JA, Coalson TS, Fischl B, Andersson JL, et al. (2013): The minimal preprocessing pipelines for the Human Connectome Project. *NeuroImage*. 80:105–124.
52. Buitrago P, Nystrom N (2021): Neocortex and Bridges-2: A High Performance AI+HPC Ecosystem for Science, Discovery, and Societal Good High Performance Computing, pp 205–219.
53. Fischl B (2012): FreeSurfer. *NeuroImage*. 62:774–781.
54. Jenkinson M, Beckmann CF, Behrens TE, Woolrich MW, Smith SM (2012): Fsl. *NeuroImage*. 62:782–790.
55. Holmes A, Levi PT, Chen YC, Chopra S, Aquino KM, Pang JC, et al. (2023): Disruptions of Hierarchical Cortical Organization in Early Psychosis and Schizophrenia. *Biol Psychiatry Cogn Neurosci Neuroimaging*. 8:1240–1250.
56. (!!! INVALID CITATION !!! (46)).
57. Petersen SE, Seitzman BA, Nelson SM, Wig GS, Gordon EM (2024): Principles of cortical areas and their implications for neuroimaging. *Neuron*. 112:2837–2853.
58. Sandhu Z, Tanglay O, Young IM, Briggs RG, Bai MY, Larsen ML, et al. (2021): Parcellation-based anatomic modeling of the default mode network. *Brain Behav*. 11:e01976.
59. Allan PG, Briggs RG, Conner AK, O'Neal CM, Bonney PA, Maxwell BD, et al. (2019): Parcellation-based tractographic modeling of the dorsal attention network. *Brain Behav*. 9:e01365.
60. Rubinov M, Kötter R, Hagmann P, Sporns O (2009): Brain connectivity toolbox: a collection of complex network measurements and brain connectivity datasets. *NeuroImage*. 47:S169.
61. Cho JW, Korchmaros A, Vogelstein JT, Milham MP, Xu T (2021): Impact of concatenating fMRI data on reliability for functional connectomics. *NeuroImage*. 226:117549.
62. Fu Z, Iraji A, Sui J, Calhoun VD (2021): Whole-Brain Functional Network Connectivity Abnormalities in Affective and Non-Affective Early Phase Psychosis. *Frontiers in Neuroscience*. Volume 15 - 2021.
63. Wang HR, Liu ZQ, Nakua H, Hegarty CE, Thies MB, Patel PK, et al. (2025): Decoding Early Psychoses: Unraveling Stable Microstructural Features Associated With Psychopathology Across Independent Cohorts. *Biological psychiatry*. 97:167–177.
64. O'Neill AG, Pax M, Parent JH, Sepulcre J, Camprodon JA, Noble S, et al. (2025): Predicting cognitive functioning in early psychosis: factors supporting and limiting generalizability of connectome-based models. *NPP—Digital Psychiatry and Neuroscience*. 3:11.

65. Meda SA, Wang Z, Ivleva EI, Poudyal G, Keshavan MS, Tamminga CA, et al. (2015): Frequency-Specific Neural Signatures of Spontaneous Low-Frequency Resting State Fluctuations in Psychosis: Evidence From Bipolar-Schizophrenia Network on Intermediate Phenotypes (B-SNIP) Consortium. *Schizophrenia bulletin*. 41:1336–1348.
66. Gohel S, Gallego JA, Robinson DG, DeRosse P, Biswal B, Szeszko PR (2018): Frequency specific resting state functional abnormalities in psychosis. *Human brain mapping*. 39:4509–4518.
67. Mueller S, Wang D, Fox MD, Yeo BT, Sepulcre J, Sabuncu MR, et al. (2013): Individual variability in functional connectivity architecture of the human brain. *Neuron*. 77:586–595.
68. Theis N, Bahuguna J, Rubin JE, Cape J, Iyengar S, Prasad KM (2024): Subject-specific maximum entropy model of resting state fMRI shows diagnostically distinct patterns of energy state distributions. *bioRxiv*.
69. Callicott JH, Mattay VS, Verchinski BA, Marenco S, Egan MF, Weinberger DR (2003): Complexity of prefrontal cortical dysfunction in schizophrenia: more than up or down. *The American journal of psychiatry*. 160:2209–2215.
70. Savin C, Tkačik G (2017): Maximum entropy models as a tool for building precise neural controls. *Curr Opin Neurobiol*. 46:120–126.
71. Gutierrez-Barragan D, Ramirez JSB, Panzeri S, Xu T, Gozzi A (2024): Evolutionarily conserved fMRI network dynamics in the mouse, macaque, and human brain. *Nat Commun*. 15:8518.
72. Corbetta M, Shulman GL (2002): Control of goal-directed and stimulus-driven attention in the brain. *Nature Reviews Neuroscience*. 3:201–215.
73. Fox MD, Corbetta M, Snyder AZ, Vincent JL, Raichle ME (2006): Spontaneous neuronal activity distinguishes human dorsal and ventral attention systems. *Proceedings of the National Academy of Sciences*. 103:10046–10051.
74. Pagani M, Gutierrez-Barragan D, de Guzman AE, Xu T, Gozzi A (2023): Mapping and comparing fMRI connectivity networks across species. *Commun Biol*. 6:1238.
75. Spreng RN, Stevens WD, Chamberlain JP, Gilmore AW, Schacter DL (2010): Default network activity, coupled with the frontoparietal control network, supports goal-directed cognition. *NeuroImage*. 53:303–317.
76. Lavigne KM, Menon M, Woodward TS (2020): Functional Brain Networks Underlying Evidence Integration and Delusions in Schizophrenia. *Schizophrenia bulletin*. 46:175–183.
77. Hur JW, Kim T, Cho KIK, Kwon JS (2021): Attenuated Resting-State Functional Anticorrelation between Attention and Executive Control Networks in Schizotypal Personality Disorder. *J Clin Med*. 10.

Supplemental Materials

S.1 Supplementary First-Order Results

The preprocessed BOLD fMRI signals from the 58 regions-of-interest, including 34 bilateral DMN and 24 bilateral DAN nodes, were compared *before z-scoring* by group **(Figure S.1.1).** There were no significant differences in any regional BOLD fMRI amplitude values within the AP fMRI acquisition, with all subjects having the same relative BOLD amplitudes. Glasser atlas regions constituting the DMN and DAN are shown in the table below **Figure S.1.1** where the DMN is the top row and the DAN is the bottom row, and all nodes are bilateral.

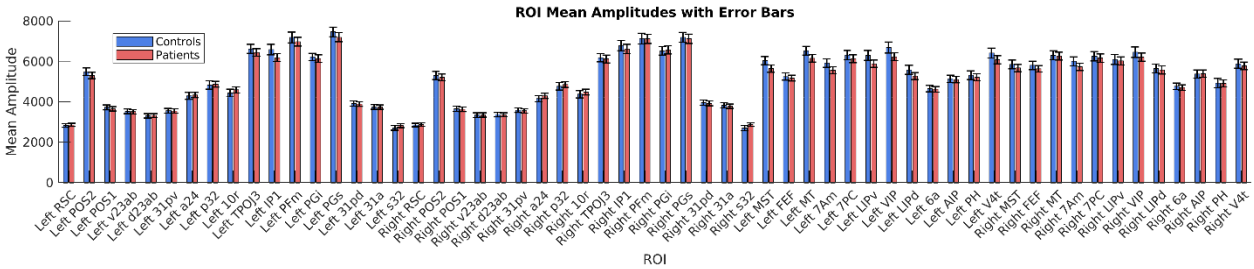

RSC	POS2	POS1	v23ab	d23ab	31pv	a24	p32	10r	TPOJ3	IP1	Pfm	PGi	PGs	31pd	31a	s32
MST	FEF	7PC	7am	LIPd	LIPv	VIP	MT	6a	AIP	PH	V4t					

Figure S1.1. Bar Region inclusion. Bar graph on top plot shows average fMRI amplitude per region in patients (red) and controls (blue). No significant differences are observed. In the table, with the DMN nodes in the top row, and DAN in the bottom row.

The DMN and DAN were examined in the context of the whole brain for the first-order frequency analysis only. For each participant, and each brain region (or node), the preprocessed fMRI timeseries (377 nodes x 410 timepoints) were analyzed using a Fourier transform. There were 360 cortical nodes and 23 subcortical nodes. Canonical resting-state frequency bands were then defined according to standard fMRI conventions: Slow 5 (0.01–0.027 Hz), Slow-4 (0.027–0.073 Hz), Slow-3 (0.073–0.198 Hz), and Slow-2 (0.198–0.50 Hz). For each subject, mean band power was extracted across these four frequency ranges for every brain region. These features were restructured into a set of features representing the average power within each brain region and frequency band and combined with demographic covariates (age, sex, group, and subject ID) to generate a comprehensive feature table. The resulting dataset was exported as a .csv file for subsequent multivariate analysis of covariance (MANCOVA). All statistical analyses on whole-brain first order band power were conducted in IBM SPSS Statistics. The tables

below contains the results for the whole-brain, frequency-band specific, first-order analyses.

A MANCOVA model with all 377 brain regions for slow-5 only was also significant (Wilk's λ=0.01, F=354.14, p=0.04). Post-hoc between-subjects' effects correcting for multiple tests using Bonferroni method showed that regional frequency band power in all four frequency bands was lower in patients compared to controls in 215 out of 377 regions. Within the DMN and DAN, 13 of the 58 regions showed significantly reduced BOLD frequency power in a MANCOVA model (Wilk's λ=0.50, F(58,104)=1.81, p=0.004; pos-thoc between-subjects' effects, Bonferroni corrected p, all<0.02) **(Figure Below).**

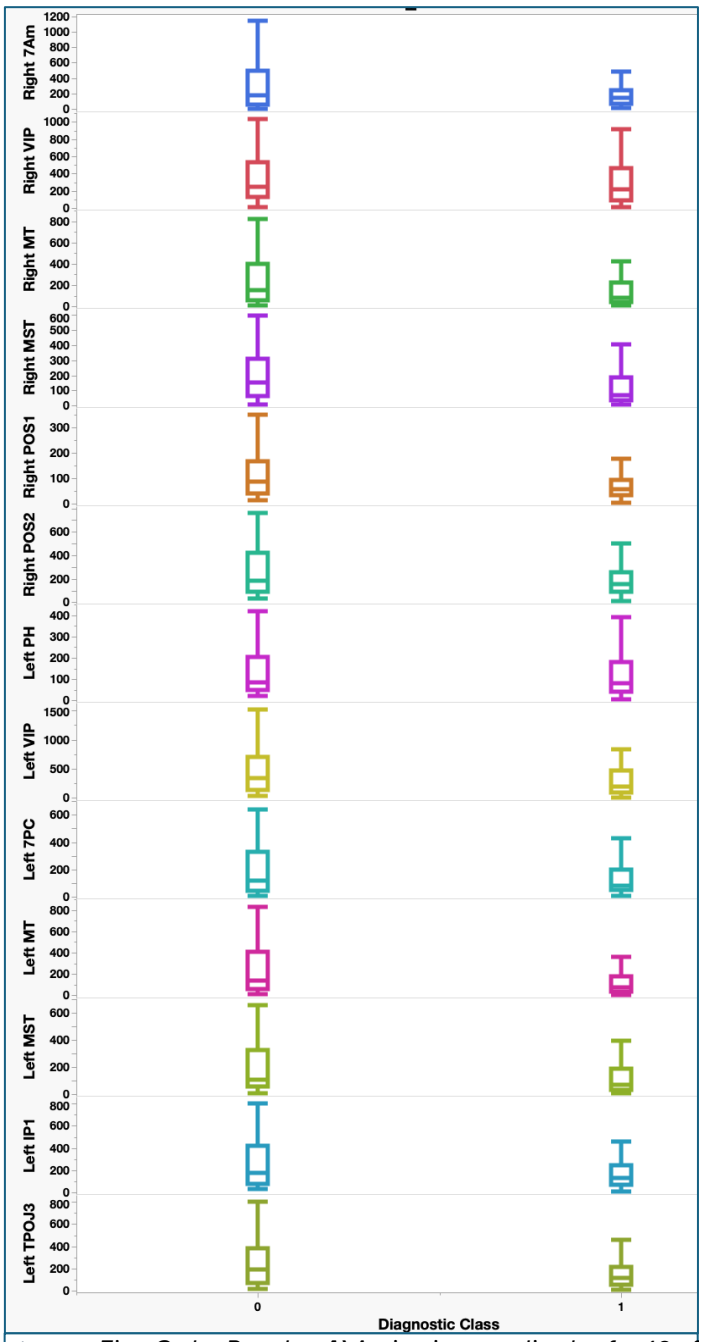

Figure 1: First Order Results. ***A)*** *Activation amplitudes for 13 of the 58 DMN and DAN regions that showed significant differences between early psychosis patients (1 on x-axis) and healthy controls (0 on x-axis). Average activation of the regions (raw BOLD signal value over time) per group are plotted in the box plots with standard error bars.*

Slow 2.

Dependent Variable	Schizophrenia Mean	Schizophrenia SD	Control Mean	Control SD	F Value	P Value	Group Diff	Cohen d
Left IFSp_Slow2	117.516	139.814	175.199	186.063	4.997	0.027	-57.683	-0.368
Left IFJa_Slow2	25.222	44.631	46.169	53.334	7.120	0.008	-20.947	-0.439
Left A5_Slow2	47.867	72.355	102.533	139.839	10.981	0.001	-54.666	-0.545
Left 7m_Slow2	369.810	458.064	607.514	940.466	4.778	0.030	-237.704	-0.359
Left IFJp_Slow2	51.819	52.160	82.879	84.454	8.479	0.004	-31.060	-0.479
Left STV_Slow2	91.617	161.179	186.877	343.616	5.884	0.016	-95.260	-0.399
Left 52_Slow2	20.963	22.980	39.505	47.568	11.424	0.001	-18.542	-0.556
Left 6r_Slow2	40.053	49.250	90.572	132.377	12.555	0.001	-50.519	-0.583
Left PFm_Slow2	44.090	50.359	68.517	81.422	5.635	0.019	-24.427	-0.390
Left 11l_Slow2	49.479	58.551	77.455	105.413	4.809	0.030	-27.976	-0.361
Left 10pp_Slow2	31.836	51.132	59.294	81.141	7.054	0.009	-27.458	-0.437
Left TE2p_Slow2	35.824	51.976	103.012	146.643	18.461	0.000	-67.188	-0.706
Left PBelt_Slow2	55.624	58.085	113.591	140.445	13.981	0.000	-57.967	-0.615
Left 5L_Slow2	117.595	181.663	216.627	336.810	6.032	0.015	-99.032	-0.404
Left 9a_Slow2	12.708	15.337	22.423	23.929	10.003	0.002	-9.715	-0.520
Left-Pallidum_Slow2	159.132	214.852	450.515	1064.998	7.600	0.007	-291.383	-0.453
Left LO3_Slow2	81.875	69.627	124.520	114.040	8.852	0.003	-42.644	-0.489
Left-Putamen_Slow2	188.708	190.841	369.721	674.007	6.832	0.010	-181.013	-0.430
Left PCV_Slow2	106.492	151.566	273.392	538.968	9.100	0.003	-166.901	-0.496
Left IFSa_Slow2	105.663	120.967	178.104	196.337	8.551	0.004	-72.440	-0.481
Right-Caudate_Slow2	197.791	356.169	356.746	552.716	4.995	0.027	-158.955	-0.367
Left PHA1_Slow2	146.200	156.621	298.653	380.655	13.198	0.000	-152.454	-0.597
Left FOP1_Slow2	83.292	90.429	123.326	130.719	5.302	0.023	-40.034	-0.379
Left V3CD_Slow2	60.161	54.425	124.581	160.869	14.355	0.000	-64.420	-0.623
Left STSda_Slow2	111.354	110.392	182.490	193.228	9.055	0.003	-71.136	-0.495
Left a10p_Slow2	80.109	88.773	155.017	195.848	11.428	0.001	-74.908	-0.556
Left AAIC_Slow2	60.523	69.059	119.833	126.897	15.143	0.000	-59.310	-0.640

Left TE1p_Slow2	14.876	17.390	25.272	33.212	6.984	0.009	-10.397	-0.434
Left 55b_Slow2	113.737	173.673	229.132	476.214	5.104	0.025	-115.395	-0.371
Left 2_Slow2	78.529	130.103	161.482	287.836	6.499	0.012	-82.953	-0.419
Left PHA3_Slow2	82.658	116.580	147.754	188.317	7.475	0.007	-65.096	-0.450
Left TE2a_Slow2	79.767	99.686	144.283	205.034	7.414	0.007	-64.515	-0.448
Left 31pv_Slow2	106.873	138.013	280.655	516.255	10.894	0.001	-173.783	-0.543
Left TE1a_Slow2	26.924	32.646	39.654	45.655	4.253	0.041	-12.730	-0.339
Left V3B_Slow2	522.945	744.709	1115.592	1527.905	11.248	0.001	-592.646	-0.551
Left STGa_Slow2	62.721	97.019	126.647	172.449	9.291	0.003	-63.925	-0.501
Left FOP2_Slow2	21.802	38.580	36.372	52.690	4.084	0.045	-14.570	-0.332
Left PFt_Slow2	57.789	73.155	86.034	83.506	5.003	0.027	-28.245	-0.368
Left FOP4_Slow2	29.292	36.993	51.271	84.327	5.406	0.021	-21.979	-0.382
Left OP2-3_Slow2	36.929	41.927	61.367	69.974	7.843	0.006	-24.438	-0.460
Left-VentralDC_Slow2	157.586	244.892	304.037	459.123	7.157	0.008	-146.451	-0.440
Brain-Stem_Slow2	144.102	186.549	378.992	933.782	6.433	0.012	-234.890	-0.417
Left 46_Slow2	54.586	59.820	93.540	139.244	6.298	0.013	-38.954	-0.413
Left 31a_Slow2	124.408	133.740	179.382	162.167	5.395	0.021	-54.974	-0.382
Left TA2_Slow2	36.984	79.421	81.949	153.953	6.142	0.014	-44.965	-0.407
Left PFop_Slow2	43.902	42.014	69.352	94.444	5.733	0.018	-25.450	-0.394
Left TF_Slow2	118.579	143.872	196.298	281.240	5.530	0.020	-77.718	-0.387
Right-Thalamus_Slow2	180.293	259.159	432.235	1071.893	5.433	0.021	-251.942	-0.383
Left MT_Slow2	45.441	80.068	90.177	168.285	5.364	0.022	-44.736	-0.381
Left PF_Slow2	31.842	47.496	50.457	55.419	5.065	0.026	-18.615	-0.370
Left TE1m_Slow2	39.776	41.848	54.905	43.609	4.699	0.032	-15.129	-0.356
Left 31pd_Slow2	23.227	25.156	35.610	50.076	4.483	0.036	-12.383	-0.348
Left A4_Slow2	14.921	16.957	21.241	20.424	4.461	0.036	-6.320	-0.347
Left 9-46d_Slow2	34.697	57.544	56.790	75.137	4.405	0.037	-22.093	-0.345
Left i6-8_Slow2	43.964	41.588	60.389	57.614	4.404	0.037	-16.425	-0.345
Left 47m_Slow2	79.292	96.632	121.462	162.971	4.343	0.039	-42.170	-0.343

Left-Hippocampus_Slow2	87.494	108.454	154.843	305.891	4.263	0.041	-67.349	-0.339

Across Slow-2 frequency bands, individuals with schizophrenia showed widespread reductions in BOLD signal amplitude across frontal, temporal, parietal, and subcortical regions relative to controls. These reductions were reflected in consistently negative group differences (−6 to −592) and medium to large effect sizes (Cohen's d ≈ −0.33 to −0.71), indicating moderate to large magnitude alterations. The largest effects emerged in auditory and temporal association cortices, including TE2p (d = −0.706; group difference = −67.19), PBelt (d = −0.615; −57.97), and V3CD (d = −0.623; −64.42), which exhibited both large absolute differences and substantial standard deviations in the control group. Frontal regions including IFJa, IFJp, IFSa, a10p, and 10pp also showed consistent reductions with moderate effect sizes (d ≈ −0.33 to −0.48) and meaningful group differences (−20 to −75). Several sensorimotor and parietal association regions, including A5, 6r, 31pv, 7m, and PFm, demonstrated similar negative shifts (d ≈ −0.36 to −0.58), reinforcing a broad reduction across large-scale cortical networks.

As for subcortical structures the Left Pallidum, Left Putamen, and Right Caudate, showed moderate negative effect sizes (d ≈ −0.37 to −0.45) paired with notably large variability in controls (SD = 1064.99 for the Left Pallidum). Limbic and paralimbic structures including (PHA1, PHA3, AAIC, and the Left Hippocampus) also displayed significant reductions (d ≈ −0.34 to −0.60), with the hippocampus showing a substantial group difference (−67.35) despite large control SDs (305). Visual region V3B has one of the largest absolute differences (−592.65), reflecting sizable reductions in schizophrenia alongside high control variability.

Across Slow-2, numerous regions reappeared in later bands (IFJa, IFJp, IFSp, 6r, A5, TE1p, TE2p), indicating frequency-generalizable abnormalities.

Slow 3.

Dependent Variable	Schizophrenia Mean	Schizophrenia SD	Control Mean	Control SD	F Value	P Value	Group Diff	Cohen d
Left IFJa_Slow3	46.163	59.770	81.339	135.581	5.342	0.022	-35.176	-0.380
Left A5_Slow3	29.123	41.816	57.003	73.036	9.720	0.002	-27.881	-0.513
Left 7m_Slow3	241.731	308.103	433.290	714.350	5.775	0.017	-191.559	-0.395
Left IFJp_Slow3	57.353	58.157	100.226	140.271	7.658	0.006	-42.873	-0.455
Left STV_Slow3	128.244	140.522	253.595	539.833	5.217	0.024	-125.352	-0.376
Left 6r_Slow3	57.010	68.745	102.088	141.557	7.599	0.007	-45.078	-0.453
Left PFm_Slow3	30.196	36.391	61.259	117.072	6.488	0.012	-31.063	-0.419
Left POS1_Slow3	220.047	233.010	333.540	406.099	5.201	0.024	-113.493	-0.375
Left 10pp_Slow3	59.322	110.101	113.791	148.462	7.095	0.009	-54.469	-0.438
Left TE2p_Slow3	40.763	62.700	71.448	102.861	5.641	0.019	-30.685	-0.390
Left 13l_Slow3	19.920	20.658	27.766	29.464	3.955	0.048	-7.846	-0.327
Left AIP_Slow3	26.850	27.231	50.004	88.676	6.307	0.013	-23.154	-0.413
Left-Cerebellum-Cortex_Slow3	168.651	222.023	355.320	654.627	7.272	0.008	-186.669	-0.443
Left PBelt_Slow3	41.555	56.730	84.980	116.415	10.404	0.002	-43.426	-0.530
Left 5L_Slow3	202.344	354.407	373.746	585.636	5.463	0.021	-171.402	-0.384
Left 9a_Slow3	48.114	57.374	90.044	113.839	9.924	0.002	-41.930	-0.518
Left FFC_Slow3	198.658	260.735	363.200	761.062	4.165	0.043	-164.542	-0.336
Left PCV_Slow3	132.642	164.587	309.626	562.701	9.286	0.003	-176.984	-0.501
Left IFSa_Slow3	80.328	66.545	146.282	174.507	12.183	0.001	-65.955	-0.574
Right-Caudate_Slow3	196.612	180.553	348.574	499.657	8.071	0.005	-151.962	-0.467
Left p9-46v_Slow3	57.470	70.587	136.735	193.333	14.606	0.000	-79.265	-0.628
Left 4_Slow3	38.637	45.221	67.958	104.840	6.281	0.013	-29.321	-0.412
Right 24dd_Slow3	14.175	14.863	21.546	17.700	7.973	0.005	-7.371	-0.464
Left PeEc_Slow3	16.377	19.208	24.810	32.935	4.309	0.039	-8.432	-0.341

Left V3CD_Slow3	58.526	88.086	91.393	107.201	4.431	0.037	-32.867	-0.346
Left STSda_Slow3	121.330	107.102	180.515	214.825	5.592	0.019	-59.185	-0.389
Left STSdp_Slow3	29.815	36.679	49.457	59.318	6.867	0.010	-19.643	-0.431
Left a10p_Slow3	62.977	82.928	126.983	212.445	7.660	0.006	-64.006	-0.455
Left AAIC_Slow3	53.528	82.750	88.642	95.609	5.985	0.015	-35.114	-0.402
Left TE1p_Slow3	15.182	20.870	23.647	25.803	5.164	0.024	-8.465	-0.374
Left PHA3_Slow3	138.356	200.750	214.285	279.355	4.022	0.047	-75.929	-0.330
Left V8_Slow3	68.631	105.088	131.526	209.709	6.605	0.011	-62.895	-0.423
Left TE1a_Slow3	35.666	43.424	77.260	109.099	12.154	0.001	-41.593	-0.573
Left FOP2_Slow3	149.105	179.809	248.817	257.336	8.404	0.004	-99.712	-0.477
Left LO2_Slow3	233.066	247.413	561.920	1139.275	8.361	0.004	-328.855	-0.475
Left PFt_Slow3	96.148	122.302	172.168	216.353	8.317	0.004	-76.020	-0.474
Left FOP4_Slow3	32.570	37.566	62.119	97.110	7.846	0.006	-29.549	-0.461
Left PoI2_Slow3	20.684	21.231	34.211	43.760	7.164	0.008	-13.526	-0.440
Right 44_Slow3	18.502	15.597	28.470	33.209	6.892	0.009	-9.968	-0.432
Right 7AL_Slow3	42.412	45.300	64.337	60.908	6.810	0.010	-21.925	-0.429
Left a9-46v_Slow3	38.927	29.327	54.320	55.267	5.477	0.020	-15.393	-0.385
Right 2_Slow3	10.416	13.437	16.253	14.177	6.726	0.010	-5.838	-0.426
Brain-Stem_Slow3	176.493	247.960	427.222	1128.742	4.941	0.028	-250.728	-0.365
Left 46_Slow3	29.665	28.546	48.918	69.483	6.322	0.013	-19.253	-0.413
Left 31a_Slow3	64.946	82.436	98.792	110.015	4.935	0.028	-33.846	-0.365
Left a32pr_Slow3	34.413	33.793	50.248	49.265	5.888	0.016	-15.835	-0.399
Left PFop_Slow3	23.165	25.190	33.502	35.827	4.631	0.033	-10.337	-0.354
Left TF_Slow3	93.151	126.754	144.700	207.368	3.908	0.050	-51.550	-0.325
Left v23ab_Slow3	102.965	123.026	197.784	389.224	5.439	0.021	-94.819	-0.383
Right-Thalamus_Slow3	533.645	766.423	885.023	1339.249	4.593	0.034	-351.377	-0.352
Left 23d_Slow3	224.503	325.852	503.115	1175.297	5.353	0.022	-278.612	-0.380
Left VMV3_Slow3	29.002	38.156	45.835	54.705	5.310	0.022	-16.834	-0.379
Right 5L_Slow3	14.493	19.933	21.878	18.747	5.283	0.023	-7.385	-0.378
Left PreS_Slow3	16.674	23.421	28.861	45.760	5.135	0.025	-12.187	-0.373

Left VMV1_Slow3	31.451	45.060	53.252	79.094	5.087	0.025	-21.800	-0.371
Left-Amygdala_Slow3	125.378	145.207	254.437	565.365	5.058	0.026	-129.059	-0.370
Left PHA2_Slow3	19.976	23.671	30.070	34.442	4.886	0.028	-10.094	-0.363
Left 31pd_Slow3	20.810	24.891	31.517	41.254	4.306	0.040	-10.707	-0.341
Left d23ab_Slow3	86.858	87.147	186.298	466.150	4.669	0.032	-99.440	-0.355
Right 24dv_Slow3	13.113	14.892	18.391	15.469	4.526	0.035	-5.278	-0.350
Left MI_Slow3	18.114	20.715	27.274	34.911	4.463	0.036	-9.160	-0.347
Right LO1_Slow3	8.688	8.603	11.653	9.732	4.016	0.047	-2.965	-0.329
Left TPOJ1_Slow3	27.169	27.506	38.498	45.216	3.986	0.048	-11.330	-0.328

Slow-3 frequency results revealed a similar but slightly more distributed pattern of broad reductions across cortical and subcortical regions in schizophrenia, with effect sizes again predominantly in the moderate range (Cohen's d ≈ −0.32 to −0.63). Several prefrontal control and association parcels exhibited some of the strongest effects, including IFSa (d = −0.574), p9-46v (d = −0.628), TE1a (d = −0.573), and Left a10p (d = −0.455), each showing sizable group differences (≈ −42 to −80). Auditory and temporal association regions including PBelt (d = −0.530), STSda (d = −0.389), STSdp (d = −0.431), a32pr (d = −0.399), and PHA3 (d = −0.330) demonstrated consistent negative differences; mirroring patterns observed in Slow-2. Parietal and sensorimotor regions, including areas 7m, 5L, 4, and 2, continued to show significant reductions with moderate effect sizes.

Looking again at subcortical regions, the Right Caudate (d = −0.467) and Right Thalamus (d = −0.352) showed significant reductions. Cerebellar cortex regions (Left and Right Cerebellum Cortex) also demonstrated moderate reductions (d ≈ −0.44 to −0.53). Notably, several visual association areas (V8, VMV1, LO2, LO1) exhibited significant reductions with medium effect sizes. The amygdala (Left Amygdala: group difference = −129.06; d = −0.370) and hippocampal-parahippocampal complex (PHA2, PHA3, PreS) again appeared consistently.

Across Slow-3, many parcels overlapped with those in Slow-2, particularly within prefrontal cortex (IFJa, IFJp, IFSa, PFm, PFt), auditory/temporal association areas (TE1a, TE1p, TE2p, STS parcels), sensory-association regions (7m, 5L, 4, POS1, PCV), and subcortical regions (Caudate, Thalamus, Pallidum). The pattern reflects stable, multimodal reductions across frontal, temporal, parietal, and subcortical systems, with several parcels showing progressively larger effect sizes moving from Slow-2 to Slow-3.

Slow 4.

Dependent Variable	Schizophrenia Mean	Schizophrenia SD	Control Mean	Control SD	F Value	P Value	Group Diff	Cohen d
Left IFJa_Slow4	57.859	54.557	117.236	153.608	13.130	0.000	-59.377	-0.596
Left A5_Slow4	48.025	52.191	90.675	144.886	7.571	0.007	-42.650	-0.452
Left STV_Slow4	176.823	275.110	341.621	518.950	7.125	0.008	-164.797	-0.439
Left 24dd_Slow4	165.608	279.759	325.049	736.649	4.003	0.047	-159.441	-0.329
Left 52_Slow4	23.700	26.430	45.654	57.392	11.326	0.001	-21.954	-0.553
Left 6r_Slow4	60.097	82.643	128.199	178.832	11.202	0.001	-68.101	-0.550
Left 10pp_Slow4	76.942	87.966	118.705	139.127	5.534	0.020	-41.763	-0.387
Left-Thalamus_Slow4	132.255	219.704	304.285	475.517	10.111	0.002	-172.030	-0.523
Right-Cerebellum-Cortex_Slow4	47.787	75.697	80.564	119.532	4.612	0.033	-32.777	-0.353
Left TE2p_Slow4	66.236	104.011	128.637	163.828	8.879	0.003	-62.402	-0.490
Left AIP_Slow4	76.488	71.509	149.990	187.426	13.113	0.000	-73.502	-0.595
Left-Cerebellum-Cortex_Slow4	140.342	190.416	333.730	713.799	7.061	0.009	-193.388	-0.437
Left PBelt_Slow4	49.740	53.790	102.837	118.317	15.706	0.000	-53.097	-0.652
Left 5L_Slow4	234.516	262.153	445.766	664.919	8.479	0.004	-211.250	-0.479
Left-Putamen_Slow4	168.746	150.933	358.804	660.070	8.243	0.005	-190.058	-0.472
Left PCV_Slow4	184.473	322.397	440.531	856.039	7.673	0.006	-256.058	-0.455
Right-Putamen_Slow4	95.631	142.919	210.869	456.667	5.855	0.017	-115.238	-0.398
Right-Caudate_Slow4	376.586	530.052	733.882	1015.351	8.844	0.003	-357.295	-0.489
Left IPS1_Slow4	201.011	291.825	324.518	415.015	4.927	0.028	-123.507	-0.365
Left p9-46v_Slow4	88.557	160.422	148.355	179.916	4.729	0.031	-59.798	-0.358
Left TGd_Slow4	36.674	28.938	58.573	70.179	8.003	0.005	-21.898	-0.465
Right 24dd_Slow4	10.302	12.676	15.431	14.030	5.628	0.019	-5.129	-0.390
Left FOP1_Slow4	116.763	105.567	159.413	132.447	5.058	0.026	-42.650	-0.370
Left PeEc_Slow4	43.877	49.567	76.772	107.380	7.254	0.008	-32.895	-0.443
Left V3CD_Slow4	61.470	77.328	97.211	97.220	6.608	0.011	-35.741	-0.423
Left-Caudate_Slow4	346.407	488.374	743.563	1270.636	8.303	0.004	-397.157	-0.474

Left STSda_Slow4	86.966	72.714	148.565	151.711	12.456	0.001	-61.599	-0.580
Left STSdp_Slow4	78.504	95.550	133.127	187.137	6.178	0.014	-54.623	-0.409
Left AAIC_Slow4	38.753	52.175	71.996	94.536	8.483	0.004	-33.242	-0.479
Left 2_Slow4	65.273	97.132	120.673	204.625	5.571	0.019	-55.400	-0.388
Left PHA3_Slow4	101.033	96.444	150.154	172.219	5.520	0.020	-49.121	-0.386
Left V8_Slow4	72.580	116.306	138.358	209.258	6.743	0.010	-65.778	-0.427
Left V6A_Slow4	22.680	23.575	34.991	34.082	7.376	0.007	-12.311	-0.447
Right-Pallidum_Slow4	47.804	76.610	97.912	162.989	7.227	0.008	-50.108	-0.442
Left-VentralDC_Slow4	62.259	79.456	119.487	240.814	5.101	0.025	-57.228	-0.371
Left STSvp_Slow4	35.779	35.958	63.852	99.973	6.894	0.009	-28.073	-0.432
Left a9-46v_Slow4	50.971	44.356	78.678	92.250	6.802	0.010	-27.707	-0.429
Left s32_Slow4	17.965	22.459	28.700	30.071	6.667	0.011	-10.734	-0.425
Brain-Stem_Slow4	155.818	315.356	354.927	894.095	4.370	0.038	-199.109	-0.344
Left 31a_Slow4	106.190	123.027	180.139	258.806	6.200	0.014	-73.949	-0.409
Left VMV3_Slow4	49.202	59.723	76.914	108.288	4.495	0.036	-27.712	-0.349
Right LIPd_Slow4	15.924	14.266	22.699	23.627	5.254	0.023	-6.775	-0.377
Left V7_Slow4	121.516	121.328	180.130	211.856	5.105	0.025	-58.614	-0.371
Right 10r_Slow4	11.078	10.619	15.869	17.483	4.774	0.030	-4.791	-0.359
Left FST_Slow4	8.422	7.822	12.167	14.225	4.769	0.030	-3.745	-0.359
Left VVC_Slow4	32.164	30.389	48.877	68.268	4.730	0.031	-16.713	-0.358
Left 31pd_Slow4	191.924	348.054	335.885	496.779	4.688	0.032	-143.962	-0.356
Left RI_Slow4	12.363	13.293	17.568	18.543	4.300	0.040	-5.205	-0.341
Right PHT_Slow4	5.869	5.213	8.211	9.508	4.183	0.042	-2.342	-0.336
Left 8Ad_Slow4	40.077	47.928	60.198	81.807	3.962	0.048	-20.121	-0.327
Left IP1_Slow4	100.191	172.985	178.819	337.435	3.927	0.049	-78.627	-0.326

Slow-4 frequency band results demonstrated reductions across cortical association, limbic, and subcortical regions, with many regions showing consistently moderate-to-large negative effect sizes (Cohen's d ≈ −0.33 to −0.65). Some of the strongest effects emerged in temporal and auditory association regions, including PBelt (d = −0.652; group difference = −53.10), TE2p (d = −0.490; −62.40), STSda (d = −0.580; −61.60), and STSdp (d = −0.409; −54.62), all of which also exhibited large control SDs (up to 187). Frontal regions including

IFJa (d = −0.596), AIP (d = −0.595), 6r (d = −0.550), and area 52 (d = −0.553) again showed substantial reductions with sizable group differences (−20 to −75).

Subcortical structures continued to show pronounced reductions. The Left Thalamus (d = −0.523), Left and Right Caudate (d = −0.47 to −0.49), Left Putamen (d = −0.472), and Right Pallidum (d = −0.442) demonstrated significant reductions accompanied by very large SDs in controls (many exceeding 400–1000). Parietal region including PCV, IPS1, and PFt showed moderate reductions (d ≈ −0.36 to −0.46). Limbic and paralimbic regions, including PHA3, AAIC, PeEc, s32, and 31a, again showed significant negative differences, paralleling abnormalities in related regions across Slow-2 and Slow-3.

Visual regions such as V3CD, V8, V6A, V7, and VVC demonstrated moderate reductions (effect sizes ≈ −0.36 to −0.43), indicating that visual network involvement continues into this frequency band. Overall, Slow4 captures frontal, temporal, and subcortical reductions that are similar to prior bands.

Slow 5.

Dependent Variable	Schizophrenia Mean	Schizophrenia SD	Control Mean	Control SD	F Value	P Value	Group Diff	Cohen d
Left IFSp_Slow5	118.790	115.368	257.281	327.408	15.771	0.000	-138.491	-0.653
Left IFJa_Slow5	48.972	49.281	104.271	152.467	11.968	0.001	-55.300	-0.569
Left d32_Slow5	180.868	221.942	382.075	539.878	11.434	0.001	-201.207	-0.556
Left A5_Slow5	61.047	68.491	119.008	152.392	11.356	0.001	-57.961	-0.554
Left 7m_Slow5	396.955	483.500	1016.504	1900.86	10.334	0.002	-619.548	-0.529
Left IFJp_Slow5	50.570	87.217	101.347	112.105	10.277	0.002	-50.777	-0.527
Left 23c_Slow5	227.494	290.324	493.772	771.801	10.213	0.002	-266.278	-0.525
Left STV_Slow5	153.187	218.596	352.528	601.895	9.552	0.002	-199.341	-0.496
Left 24dd_Slow5	96.271	152.569	268.412	558.301	9.090	0.003	-172.141	-0.508
Left 52_Slow5	26.560	34.993	49.193	63.504	8.724	0.004	-22.633	-0.486
Left 6r_Slow5	58.290	82.960	128.505	222.329	8.587	0.004	-70.215	-0.482
Left PFm_Slow5	28.141	33.099	48.299	57.476	8.167	0.005	-20.158	-0.470
Left POS1_Slow5	211.636	294.644	384.971	500.790	7.819	0.006	-173.334	-0.460
Left 11l_Slow5	39.625	61.578	74.841	101.340	7.675	0.006	-35.216	-0.455
Left 10pp_Slow5	118.176	191.917	221.225	283.569	7.623	0.006	-103.049	-0.454
Left-Thalamus_Slow5	68.742	99.706	143.289	246.083	7.609	0.006	-74.547	-0.454
Right-Cerebellum-Cortex_Slow5	37.626	58.734	78.384	131.027	7.607	0.006	-40.758	-0.453
Left TE2p_Slow5	87.133	115.209	162.410	235.836	7.606	0.006	-75.277	-0.453
Left 13l_Slow5	15.352	19.670	26.406	31.664	7.602	0.006	-11.054	-0.453
Left AIP_Slow5	112.825	100.124	172.481	183.880	7.293	0.008	-59.656	-0.444
Left-Cerebellum-Cortex_Slow5	106.919	171.543	272.283	597.503	7.228	0.008	-165.364	-0.442
Left 7Pm_Slow5	126.381	204.107	274.059	506.080	7.076	0.009	-147.678	-0.437
Left PBelt_Slow5	65.587	110.154	122.331	162.516	7.027	0.009	-56.744	-0.436
Left 5L_Slow5	325.042	375.179	615.101	1050.03	6.689	0.011	-290.059	-0.425
Left 9a_Slow5	20.407	21.129	37.442	62.428	6.664	0.011	-17.035	-0.424
Left 10v_Slow5	15.833	17.369	24.769	27.027	6.619	0.011	-8.936	-0.423

Left-Pallidum_Slow5	276.667	327.703	525.568	906.985	6.572	0.011	-248.901	-0.421
Left STSva_Slow5	17.439	16.720	25.985	26.168	6.491	0.012	-8.546	-0.419
Left FFC_Slow5	216.041	268.036	349.247	419.624	6.134	0.014	-133.206	-0.407
Left LO3_Slow5	121.787	120.385	172.487	137.564	5.948	0.016	-50.700	-0.401
Left-Putamen_Slow5	291.529	324.128	479.810	669.327	5.940	0.016	-188.282	-0.401
Left PCV_Slow5	159.419	265.248	333.736	651.496	5.922	0.016	-174.317	-0.400
Right d23ab_Slow5	30.566	23.997	41.894	35.805	5.831	0.017	-11.328	-0.397
Right-Putamen_Slow5	95.126	156.825	189.208	346.955	5.753	0.018	-94.082	-0.394
Left IFSa_Slow5	73.601	108.016	121.640	147.791	5.654	0.019	-48.039	-0.391
Right-Caudate_Slow5	245.989	289.644	400.190	549.264	5.589	0.019	-154.201	-0.389
Left IPS1_Slow5	210.492	424.436	464.670	957.380	5.576	0.019	-254.178	-0.388
Left PHA1_Slow5	49.658	54.700	73.143	70.599	5.568	0.019	-23.485	-0.388
Left p9-46v_Slow5	107.295	121.570	166.448	201.346	5.515	0.020	-59.152	-0.386
Left LO1_Slow5	49.787	66.755	117.118	287.349	5.443	0.021	-67.331	-0.384
Left PoI1_Slow5	51.585	77.098	85.233	108.802	5.280	0.023	-33.647	-0.378
Left 4_Slow5	63.368	95.185	111.788	176.800	5.241	0.023	-48.420	-0.376
Left TGd_Slow5	47.725	45.082	73.458	99.690	5.213	0.024	-25.734	-0.375
Right 24dd_Slow5	15.716	15.227	21.497	15.933	5.165	0.024	-5.780	-0.374
Left PHT_Slow5	49.730	69.678	111.184	269.065	5.054	0.026	-61.455	-0.370
Left FOP1_Slow5	68.944	95.856	104.254	98.240	4.936	0.028	-35.310	-0.365
Left PeEc_Slow5	34.378	42.824	60.546	108.395	4.891	0.028	-26.168	-0.364
Left V3CD_Slow5	39.115	50.212	61.130	77.156	4.873	0.029	-22.015	-0.363
Left-Caudate_Slow5	159.408	183.651	250.513	348.562	4.848	0.029	-91.105	-0.362
Left STSda_Slow5	25.064	33.464	45.832	87.417	4.805	0.030	-20.768	-0.360
Left STSdp_Slow5	105.000	150.119	170.902	238.891	4.699	0.032	-65.902	-0.356
Left a10p_Slow5	68.748	70.258	103.271	136.552	4.611	0.033	-34.522	-0.353
Left AAIC_Slow5	45.090	49.882	64.793	66.696	4.559	0.034	-19.702	-0.351
Left TE1p_Slow5	21.477	21.723	31.101	36.522	4.492	0.036	-9.624	-0.348
Left 55b_Slow5	76.097	112.749	255.656	875.489	4.466	0.036	-179.559	-0.347
Left 25_Slow5	14.384	17.991	23.805	39.304	4.462	0.036	-9.421	-0.347

Left 2_Slow5	74.201	127.076	122.044	159.673	4.387	0.038	-47.844	-0.344
Left 24dv_Slow5	42.812	76.063	73.008	109.367	4.286	0.040	-30.196	-0.340
Left 8Av_Slow5	68.072	76.474	97.081	103.668	4.150	0.043	-29.009	-0.335
Left PHA3_Slow5	18.322	14.113	24.044	21.914	4.121	0.044	-5.723	-0.334
Left TE2a_Slow5	75.953	109.955	119.517	163.753	4.116	0.044	-43.564	-0.334
Left 31pv_Slow5	75.074	66.099	112.037	171.644	3.938	0.049	-36.964	-0.328

Tables S1. All significant results from brain-wide, group-wise, power band analysis.

Across Slow-5, schizophrenia participants again exhibited large, diffuse reductions spanning frontal, temporal, parietal, limbic, visual, cerebellar, and subcortical regions, with Cohen's d values ranging from −0.32 to −0.65. Some of the strongest effects in this lowest-frequency band appeared in frontal regions including IFSp (d = −0.653; group difference = −138.49), IFJa (d = −0.569; −55.30), d32 (d = −0.556; −201.21), 7m (d = −0.529; −619.55), IFJp (d = −0.527; −50.78), and 23c (d = −0.525; −266.28). These regions showed large absolute differences and high standard deviations in the control group, indicating substantial variability but consistent reductions across participants with schizophrenia.

Temporal and auditory regions such as STV (d = −0.496), STSva (d = −0.419), STSda (d = −0.360), STSdp (d = −0.356), TE2p (d = −0.453), TE2a (d = −0.334), TE1p (d = −0.348), and PHT (d = −0.370) again demonstrated strong involvement, mirroring patterns in all prior bands. Subcortical structures including the Left Pallidum (d = −0.421), Left Putamen (d = −0.401), Right Putamen (d = −0.394), Left Caudate (d = −0.362), and Right Caudate (d = −0.389) continued to display moderate reductions with very large SDs (300–900).

Parietal association regions (A5, 5L, IPS1, PCV, POS1) again showed consistent negative differences (d = −0.38 to −0.46), along with cerebellar cortex regions (Left and Right Cerebellum Cortex), which showed pronounced reductions (d = −0.44 to −0.45). Limbic areas including PHA1, PHA3, AAIC, 25, 24dv, and a10p also demonstrated moderate reductions, contributing to a cross-frequency pattern of paralimbic involvement. Visual regions (LO1, LO3, V3CD, V8, VMV3, VVC) similarly showed significant effects, indicating that visual association cortex consistently exhibits low-frequency reductions across bands.

Across all frequency bands, Slow-5 showed the strongest and most widespread effects, with numerous regions showing their largest Cohen's d values in this band (IFSp, d32, 7m, 23c). The substantial overlap of regions across Slow2–5, especially within frontal, temporal, auditory, and parietal regions demonstrates stable, frequency-generalizable reductions in schizophrenia, with Slow-5 reflecting the most pronounced distributed disruptions.

S.2 Supplementary Second-Order Results

Of the 816 unique edges that represent the direct connections between DMN and DAN, at the individual level, there were more negatively weighted edges in the patient group (on average 129 per patient) than the control group (approximately 74 per person). Among patients, the average minimum edge weight for an edges between DMN and DAN was r =–0.39 (±0.195), compared to r= –0.21 (±0.192) among controls. A two-sample KS-test comparing the FC edge-weight distributions between patients and controls indicated patients have significantly more negative correlations (main text **Figure 2D,E**; KS =.324, p<.001), although the standard deviations were very large in both groups (patients: 196±140 negatively weighted edges; controls: 104±92).

Regarding graph metrics, a summary of the relevant findings from the main text goes as follows: Patients showed lower average clustering coefficient in the DMN+DAN(t = -3.34, p = .0011), DMN (t = -3.34, p = .0010), and DAN (t = -2.80, p = .0057), and the same findings were observed for efficiency: DMN+DAN(t = -3.33, p = .0011), DMN (t = -3.27, p = .0013), and DAN (t = -2.82, p = .0054). Modularity coefficient was significantly higher among patients in the DMN+DAN (t = 2.83, p=.0052) and the DMN (t=3.133, p=.0020), but not in the DAN. Average betweenness centrality was only significantly different in the DMN+DAN network (t = 2.83, p = .0053), but group differences were not found in either DMN or DAN alone for average betweenness centrality.

The four canonical frequency bands described above (slow-5, slow-4, slow-3, and slow-2) were applied as bandpass filters to the preprocessed timeseries frequency domain data. Then, the filtered frequency domains were inverse Fourier transformed back into the time domain, creating four band-filtered timeseries per region and per subject. Next, the functional connectomes were created for the 58-node DMN+DAN for each frequency band. The same graph measures were then calculated for the frequency-band specific functional connectomes as were calculated for the full-spectrum FC shown in the main text. Groupwise (patient-control) differences were then examined using two-sample t-test for each measure.

Group-level average FC networks for each frequency band are shown in **Supplemental Figure 1.** Visibly, the FC correlations are weaker across the board for both patients and controls at higher frequencies. **A table of graph measure difference** are is provided in **Supplemental Table 2.** The results are very consistent with full spectrum FC, and all significant differences are in the same direction as the full spectrum FC. Some graph properties can be localized to specific bands.

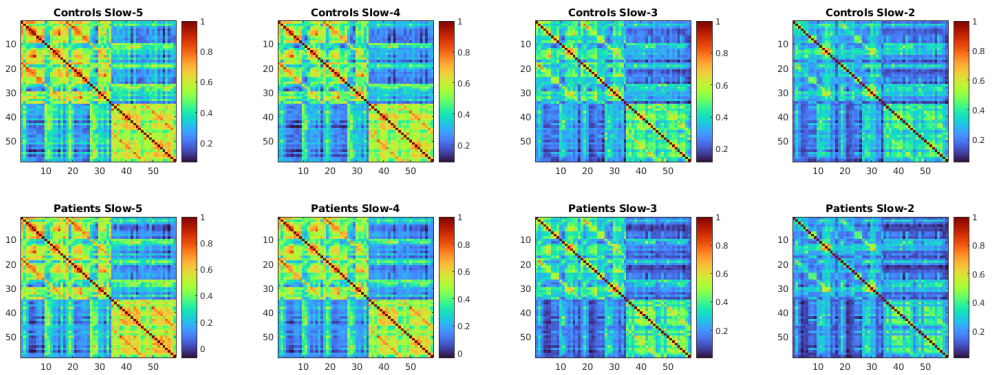

Figures S1. The frequency-band-specific FC group level averages. Top row: controls; bottom row: patients. From left to right: slow-5, slow-4, slow-3, slow-2. Nodal order is the same as in the main manuscript (DMN is upper left block, DAN is lower right). Inter-network connections are in the off diagonal blocks.

	Measure	Mean Patients	SD Patients	Mean Controls	SD Controls	T value	p Value
Slow-5	Clustering	0.42	0.111	0.48	0.129	*-3.03	0.0029
	Modularity	0.18	0.424	0.13	0.049	1.88	0.0618
	Efficiency	0.52	0.080	0.56	0.091	*-2.99	0.0032
	Betweenness	46.73	19.170	34.08	18.046	*4.01	9.3391e-05
Slow-4	Clustering	0.37	0.128	0.42	0.125	*-2.31	0.0222
	Modularity	0.17	0.061	0.15	0.059	*2.07	0.0396
	Efficiency	0.45	0.093	0.49	0.090143	*-2.99	0.0230
	Betweenness	60.27	30.818	45.17	25.519	*4.01	0.0019
Slow-3	Clustering	0.29	0.098	0.37	0.105	*-4.75	4.4887e-06
	Modularity	0.17	0.051	0.13	0.049	*4.40	1.9336e-05
	Efficiency	0.36	0.077	0.42	0.080	*-4.55	1.0568e-05
	Betweenness	76.13	35.009	58.78	29.048	*3.19	0.0017
Slow-2	Clustering	0.26	0.101	0.30	0.109	*-2.37	0.0191
	Modularity	0.14	0.043	0.13	0.049	1.26	0.2081
	Efficiency	0.33	0.087	0.36	0.089	*-2.37	0.0187
	Betweenness	39.73	24.926	44.72	26.924	-1.18	0.2380

Table S2 DMN+DAN. The frequency-band-specific FC graph metric comparison results for DMN+DAN (58 nodes).

	Measure	Mean Patients	SD Patients	Mean Controls	SD Controls	T value	p Value
Slow-5	Clustering	0.50	0.131	0.56	0.130	*-3.02	0.0030

	Modularity	0.12	0.043	0.10	0.044	*2.63	0.0094
	Efficiency	0.56	0.096	0.61	0.095	*-3.06	0.0029
	Betweenness	19.60	10.804	14.58	9.421	*2.94	0.0037
Slow-4	Clustering	0.47	0.127	0.50	0.110	-1.44	0.1508
	Modularity	0.11	0.041	0.10	0.033	1.17	0.2454
	Efficiency	0.514	0.096	0.53	0.080	-1.35	0.1775
	Betweenness	20.52	10.933	17.64	9.046	1.63	0.0925
Slow-3	Clustering	0.36	0.107	0.43	0.099	*-4.03	8.5547e-05
	Modularity	0.13	0.043	0.106	0.038	*3.56	0.0005
	Efficiency	0.40	0.085	0.45	0.077	*-3.947	0.0001
	Betweenness	28.72	13.697	24.75	12.643	1.81	0.0724
Slow-2	Clustering	0.28	0.112	0.32	0.096	*-2.31	0.0219
	Modularity	0.15	0.052	0.14	0.044	*2.54	0.0121
	Efficiency	0.32	0.94	0.36	0.079	*-2.33	0.0210
	Betweenness	14.73	12.652	18.69	10.510	*-2.01	0.0461

Table S2 DMN. The frequency-band-specific FC graph metric comparison results for DMN only (34 nodes).

	Measure	Mean Patients	SD Patients	Mean Controls	SD Controls	T value	p Value
Slow-5	Clustering	0.58	0.151	0.62	0.157	-1.86	0.0653
	Modularity	0.10	0.051	0.09	0.048	1.52	0.1309
	Efficiency	0.61	0.113	0.64	0.118	-1.70	0.0905
	Betweenness	11.46	8.880	8.69	1.866	1.75	0.0822
Slow-4	Clustering	0.53	0.138	0.60	0.144	*-2.86	0.0047
	Modularity	0.10	0.042	0.09	0.041	*2.38	0.0186
	Efficiency	0.55	0.108	0.60	0.116	*-2.83	0.0053
	Betweenness	11.7	7.822	8.22	6.051	*2.91	0.0041
Slow-3	Clustering	0.43	0.114	0.50	0.125	*-3.66	0.0003
	Modularity	0.013	0.048	0.10	0.045	*2.82	0.0054
	Efficiency	0.45	0.091	0.51	0.100	-*-3.70	0.0003
	Betweenness	16.46	8.950	15.42	12.345	0.62	0.5343
Slow-2	Clustering	0.37	0.124	0.42	0.149	*-2.34	0.0202
	Modularity	0.14	0.054	0.12	0.055	1.81	0.0726
	Efficiency	0.40	0.106	0.44	0.124	*-2.29	0.0232
	Betweenness	11.74	9.769	11.41	8.652	0.21	0.8328

Table S2 DAN. The frequency-band-specific FC graph metric comparison results for DAN only (24 nodes).

S.3 Supplementary MEM results

MEMs were fit using the maximum likelihood estimation (MLE). The MLE is an iterative method that runs until convergence and determines values of *J* and *h*, the interaction coefficient and the activation bias, respectively, for each system. Once fit, the theoretical probability of a brain state can be calculated from the model parameters, *J* and *h*. This theoretical probability is defined for each unique brain state and is the expected rate of occurrence (in the whole population) of that state. Correlating the theoretical probability to the actual observed (sometimes called empirical) probability of the states demonstrates how well the MLE algorithm performed, i.e. how well the MEM explains the data. As shown in **Supplemental Figure 2**, all models had excellent fits (r > .99, p < .001).

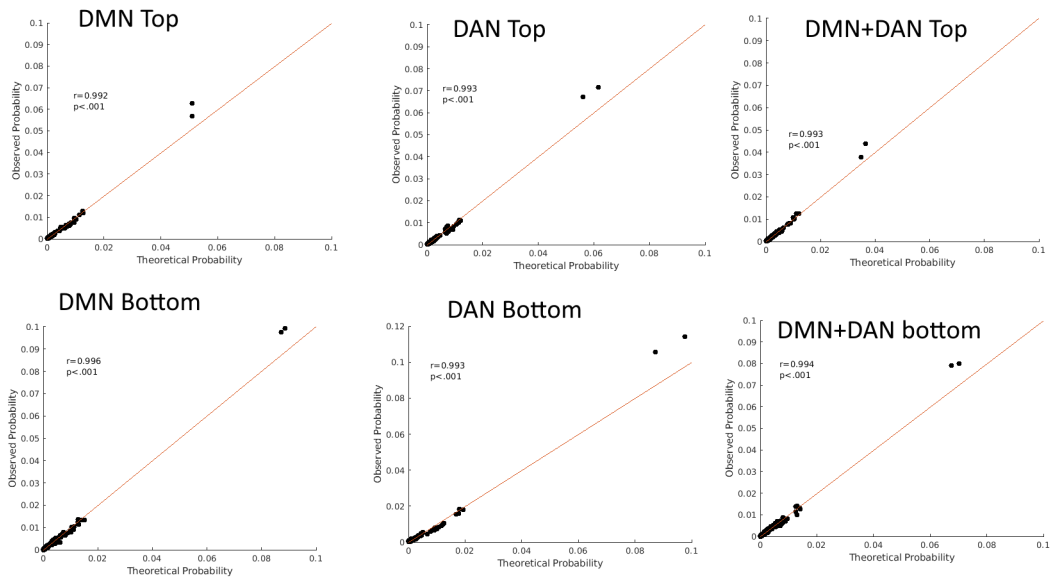

Supplemental Figure 2. Scatter plots for whole-population MEM fit results. The x-axis shows the theoretical probability, the y-axis the observed probability. Scatter points are unique brain states. The red line is the linear least-squared squared line. All correlations are highly significant (r >. 99, p < .001).

We examined differences in MEM metrics among non-affective psychosis, affective psychosis patients, and controls using MANCOVA that showed a trend toward significance (Wilk's λ=0.72, F=1.42, p=0.051). Post-hoc between-subjects' effects for MEM metrics with Bonferroni corrections showed a similar pattern of significant differences in MEM metrics as psychosis-control comparison except for bottom distinct states showing a trend toward significance (p=0.08). Another pos-thoc test to compare NAP, AP, and controls, showed that all MEM metrics with significant differences in the between-subjects' effects tests were different between controls and NAP but not between controls and AP except top energy trace, which was the highest in NAP, intermediate in AP and the lowest in controls after Games-Howell corrections for multiple testing.

Between NAP and AP patients, no differences in the distributions of distinct states were found in any of the six systems. Between NAP and controls, differences were seen in every system (DMN-top: KS=0.33, p=0.001; DMN-bottom: KS=0.31, p=0.002; DAN-top: KS=0.30, p=0.003; DAN-bottom: KS=0.33, p-0.001; DMN+DAN-top: KS=0.34, p<0.001; DMN+DAN-bottom: KS=0.33, p<0.001). Between AP and controls, significant differences were observed in three systems (DMN-bottom: KS=0.32,p=0.037; DAN-top: KS=0.37, p=0.012; DMN-DAN-top: KS=0.448, p<0.001).

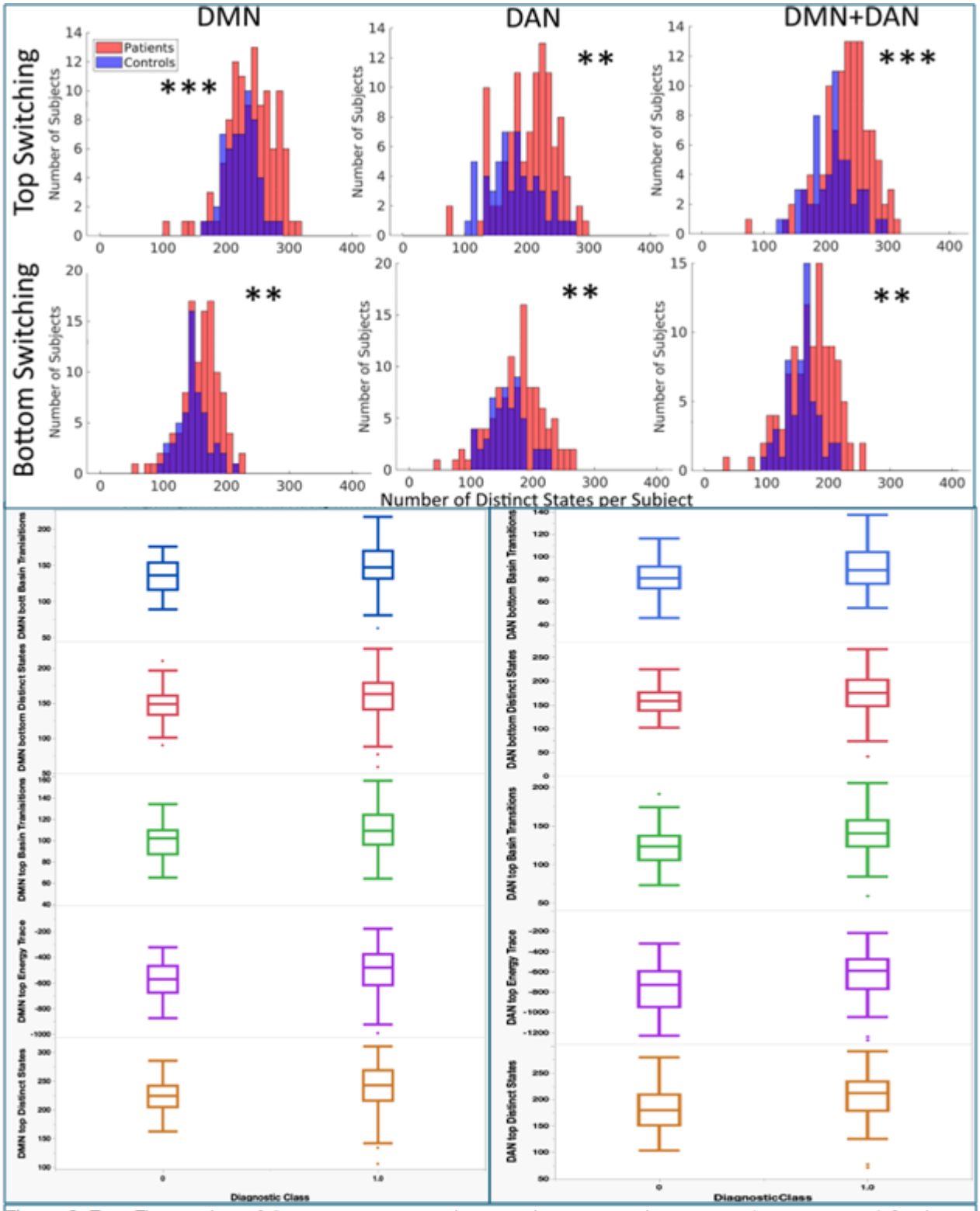

Figure 3: Top: The number of distinct states per subject is shown in two histograms (one per group) for the six systems. Asterisks indicate significance of difference of distribution by 2-sample KS-test (**p<0.01; ***p<0.001). Bottom: Differences in MEM metrics for DMN and DAN observed using MANCOVA model. Observed significances are corrected for multiple tests using Bonferroni approach (DMN+DAN differences are in supplemental information).

Permutation tests were conducted for the DMN, DAN, and DMN+DAN. In each case, the selection of nodes was being permuted over 500 instances. In each instance, for a given case (say, DMN), 10 nodes are randomly selected from the system. Next, this node set (permutation) is fit using the same MEM approach described in **Section 2.4** of the main text.

For each permutation, the MEM "summary variables" assessed in the main text, namely number of distinct states, energy trace, and number of basin transitions in the energy landscape are calculated for each participant. Then, group-level differences in the distribution of each variable are assessed by two-sample KS-test. This provides a distribution over 500 permutations of the group level differences of the summary variables, for each system (**Figures Below).**

Results are summarized as follows: for the DMN, patients had more distinct states in 99% of permutations, higher energy trace in 96%, and more basin transitions in 96%. For the DAN, 96% of permutation had more distinct states, 65% had higher energy trace, and 77% of permutations had significantly more basin transitions in patients. For the combined DMN+DAN systems, across permutations, 99% show more distinct states for patients, 95% higher energy trace, and 96% had more basin transitions in the patient group. This corresponds to the results seen in the main text where for patients, all systems had more unique states (and permutations are roughly 96-99% likely to demonstrate this property), some systems had higher energy traces for patients (and only 65% of DAN permutations demonstrate this property), and transitions difference fall in-between (roughly 77-96%).

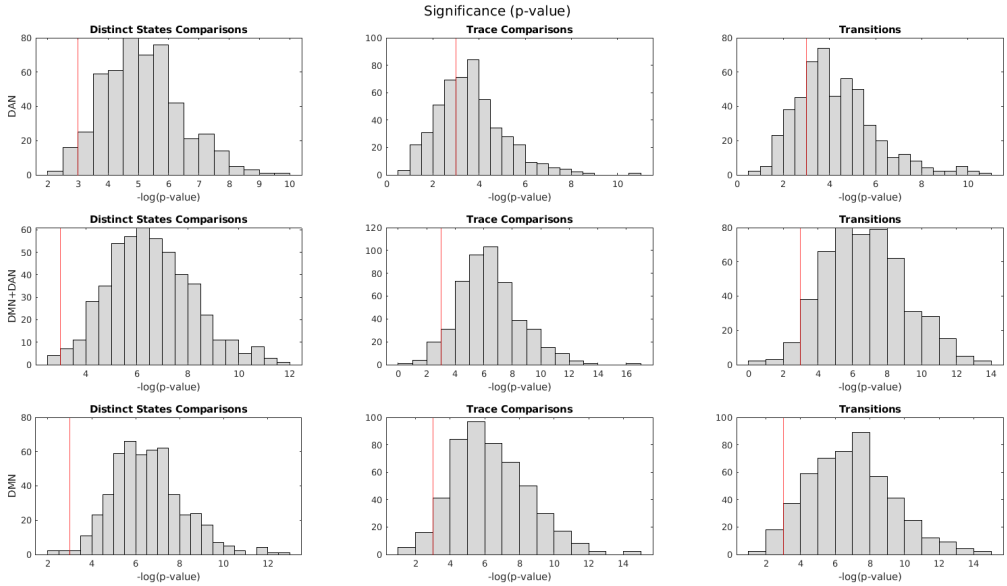

Permutation Figure (significance). In the above histograms, across the nine subplots, the rows represent the systems, which are, from top to bottom: DAN, DMN+DAN, and DMN. Column represent summary measures, which are, from left to right: distinct states, trace, and transitions. Histograms represent 500 permutations, showing the negative log likelihood of the p-value, with the red vertical line indicate the corresponding value of alpha=0.05, and more significant values lie to the right of the red line.

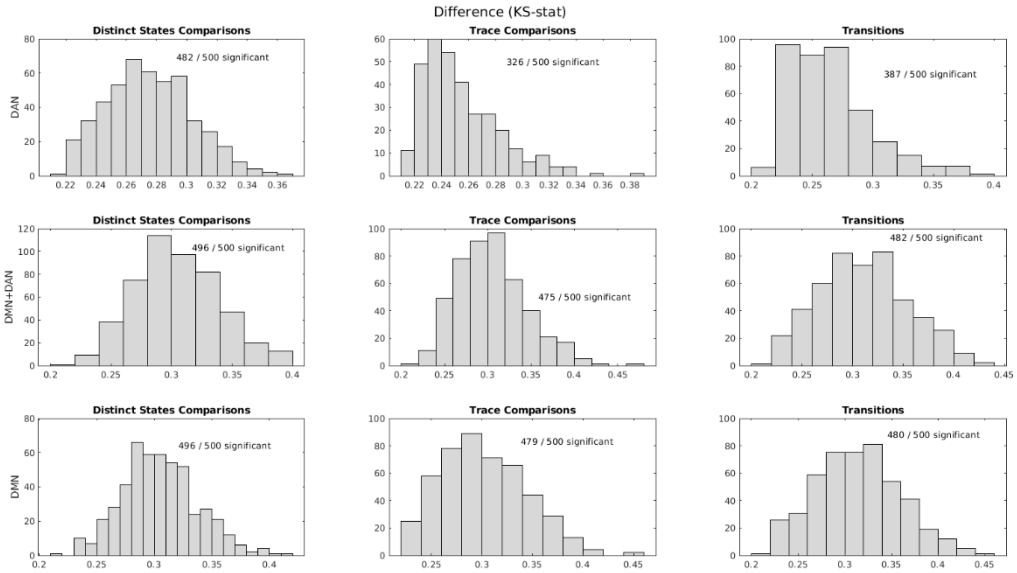

Permutation Figure (KS-statistic). In the above histograms, across the nine subplots, the rows represent the systems, which are, from top to bottom: DAN, DMN+DAN, and DMN. Column represent summary measures, which are, from left to right: distinct states, trace, and transitions. Histograms represent 500 permutations, showing the distribution of KS-statistics.

S.4 Non-Affective Psychosis versus Affective Psychosis

The non-affective psychotic (NAP) disorders are considered to be schizophrenia, schizoaffective, schizophreniform, delusional, brief psychotic disorder, and psychosis not otherwise specified. The affective psychotic (AP) disorders are considered to be major depressive and Bipolar disorder. Many of the MEM comparisons evaluated in the main text were also examined for differences between NAP and AP.

We examined differences in all MEM metrics among non-affective psychosis (NAP), affective psychosis (AP) patients, and controls using MANCOVA that showed a trend toward significance (Wilk's λ=0.72, F=1.42, p=0.051). Posthoc between-subjects' effects for MEM

metrics with Bonferroni corrections showed a similar pattern of significant differences in MEM metrics as psychosis-control comparison except for bottom distinct states showing a trend toward significance (p=0.08). Another posthoc test to compare NAP, AP, and controls, showed that all MEM metrics with significant differences in the between-subjects' effects tests were different between controls and NAP but not between controls and AP except top energy trace, which was the highest in NAP, intermediate in AP and the lowest in controls after Games-Howell corrections for multiple testing.

Between NAP and AP patients, no differences in the distributions of distinct states were found in any of the six systems. Between NAP and controls, differences were seen in every system (DMN-top: KS=0.33, p=0.001; DMN-bottom: KS=0.31, p=0.002; DAN-top: KS=0.30, p=0.003; DAN-bottom: KS=0.33, p-0.001; DMN+DAN-top: KS=0.34, p<0.001; DMN+DAN-bottom: KS=0.33, p<0.001). Between AP and controls, significant differences were observed in three systems (DMN-bottom: KS=0.32,p=0.037; DAN-top: KS=0.37, p=0.012; DMN-DAN-top: KS=0.448, p<0.001).

Between NAP and AP patients, no differences in the distributions of energy trace were found in any of the six systems. But there were differences between NAP and controls in two systems (DAN-top: KS=0.35, p<0.001; DMN+DAN-top: KS=0.34, p<0.001). Between AP and controls, DMN-DAN-top energy trace showed significant differences (KS=0.32, p<0.038).

Between NAP and AP patients, and between AP and controls, no differences in the distributions of basin transitions states were found in any of the six systems. Between NAP and controls, differences were observed in every system (DMN-top: KS=0.36, p<0.001; DAN-top: KS=0.35,p<0.001; DMN+DAN-top: KS=0.38, p<0.001; DMN+DAN-bottom: KS=0.36, p<0.001) after correcting for multiple tests.

S.5 Supplementary Energy Landscape Results

Basin transition rates for all systems are shown below. For each system, a top graph shows the basin transition matrix, and the bottom graph the basin configurations, where the lowest energy basin in the 1st basin in each transition matrix. In each basin transition matrix, each row sums to 100%, and the columns represent time *t*, while the rows represent time *t+1*. In each basin configuration plot, the lowest energy is the red basin (colors do not correspond to similar basins between systems; colors just offer a way to identify basins within a system). For each node along the a-axis, black represents "off" while white represents "on."

It is clear that while the patients have more transitions between basins (as shown in the main text), they do not have different basin transition rates for any of the basins, shown

below. In the case of the top switching DMN+DAN, basins 1 and 2 represent states of synchronized DMN+DAN activity, whereas basins 3 and 4 represented asynchrony. Interestingly, for both patients and controls, direct transitions from the DMN+DAN asynchronous basins (3 and 4) is very low (4%), whereas direct transitions from either asynchronous state to a synchronized state are comparatively high (20%).

Top DMN

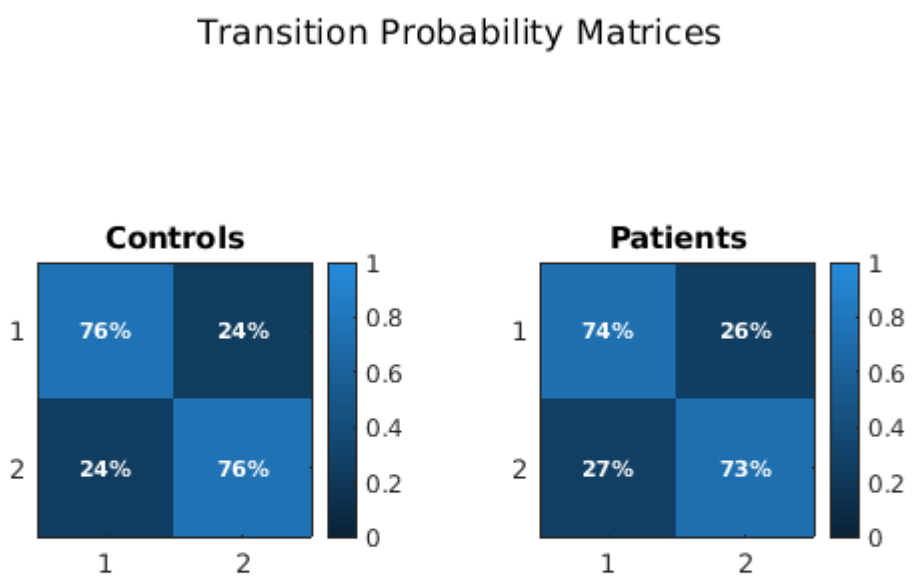

Bottom DMN

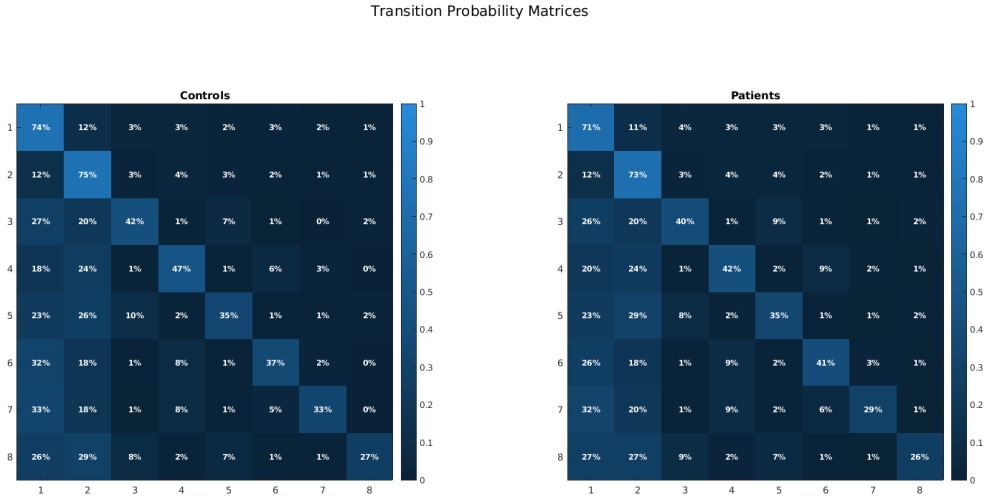
Transition Probability Matrices
Controls
1 74% 12% 3% 3% 2% 3% 2% 1%
2 12% 75% 3% 4% 3% 2% 1% 1%
3 27% 20% 42% 1% 7% 1% 0% 2%
4 18% 24% 1% 47% 1% 6% 3% 0%
5 23% 26% 10% 2% 35% 1% 1% 2%
6 32% 18% 1% 8% 1% 37% 2% 0%
7 33% 18% 1% 8% 1% 5% 33% 0%
8 26% 29% 8% 2% 7% 1% 1% 27%
1 2 3 4 5 6 7 8
1 0.9 0.8 0.7 0.6 0.5 0.4 0.3 0.2 0.1 0
Patients
1 71% 11% 4% 3% 3% 3% 1% 1%
2 12% 73% 3% 4% 4% 2% 1% 1%
3 26% 20% 40% 1% 9% 1% 1% 2%
4 20% 24% 1% 42% 2% 9% 2% 1%
5 23% 29% 8% 2% 35% 1% 1% 2%
6 26% 18% 1% 9% 2% 41% 3% 1%
7 32% 20% 1% 9% 2% 6% 29% 1%
8 27% 27% 9% 2% 7% 1% 1% 26%
1 2 3 4 5 6 7 8
1 0.9 0.8 0.7 0.6 0.5 0.4 0.3 0.2 0.1 0

Top DAN

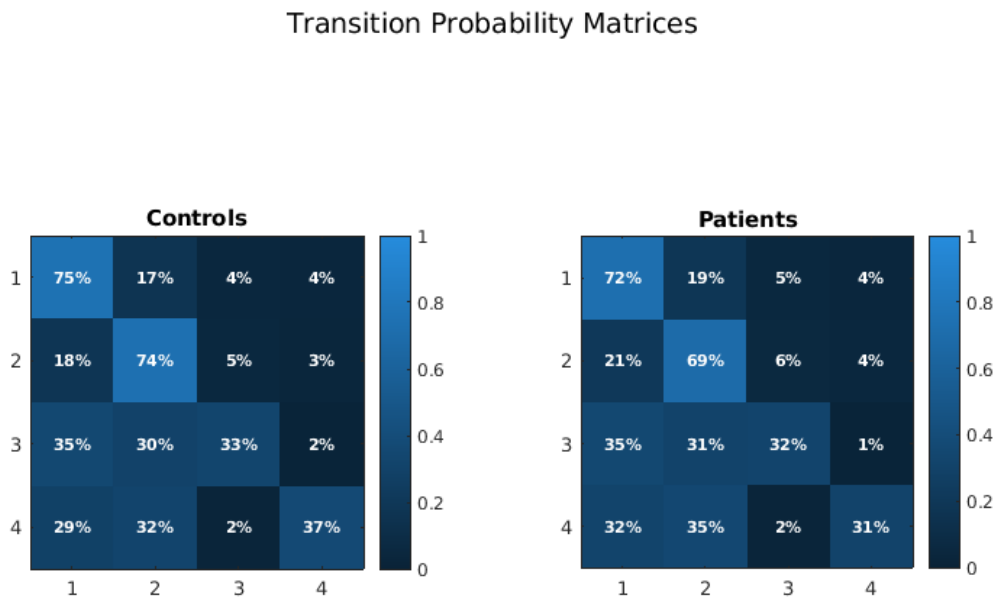
Transition Probability Matrices
Controls
1
2
3
4
75%
17%
4%
4%
18%
74%
5%
3%
35%
30%
33%
2%
29%
32%
2%
37%
1
2
3
4
1
0.8
0.6
0.4
0.2
0
Patients
1
2
3
4
72%
19%
5%
4%
21%
69%
6%
4%
35%
31%
32%
1%
32%
35%
2%
31%
1
2
3
4
1
0.8
0.6
0.4
0.2
0

Bottom DAN

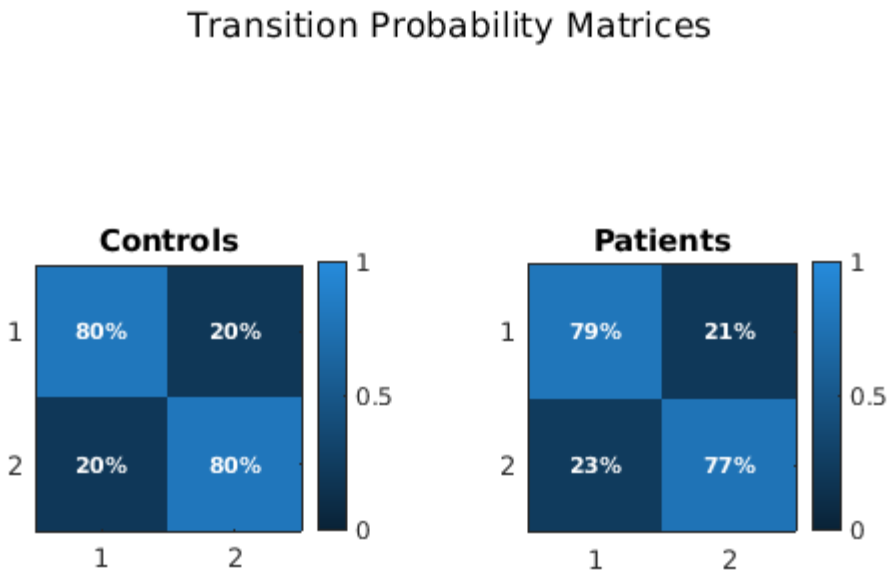
Transition Probability Matrices
Controls
80%
20%
20%
80%
1
2
1
2
1
0.5
0
Patients
79%
21%
23%
77%
1
2
1
2
1
0.5
0

Top DMN+DAN

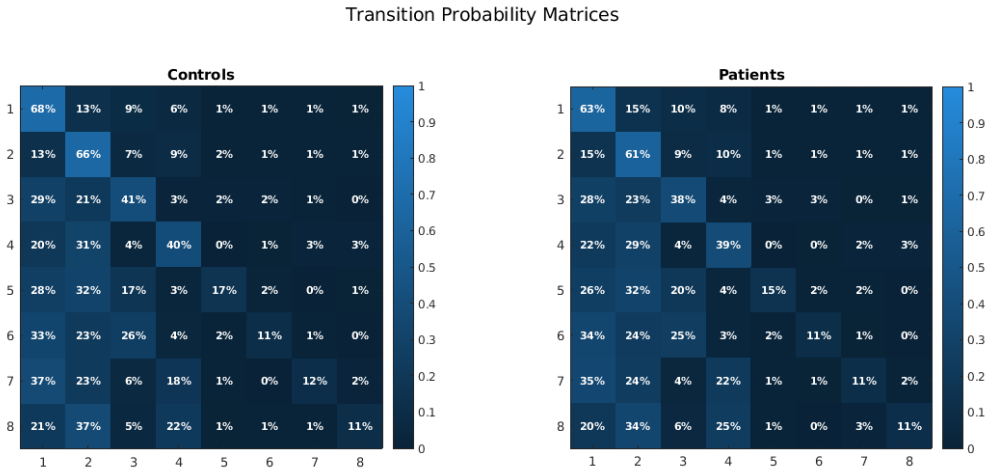
Transition Probability Matrices
Controls
1 68% 13% 9% 6% 1% 1% 1% 1%
2 13% 66% 7% 9% 2% 1% 1% 1%
3 29% 21% 41% 3% 2% 2% 1% 0%
4 20% 31% 4% 40% 0% 1% 3% 3%
5 28% 32% 17% 3% 17% 2% 0% 1%
6 33% 23% 26% 4% 2% 11% 1% 0%
7 37% 23% 6% 18% 1% 0% 12% 2%
8 21% 37% 5% 22% 1% 1% 1% 11%
1 2 3 4 5 6 7 8
1 0.9 0.8 0.7 0.6 0.5 0.4 0.3 0.2 0.1 0
Patients
1 63% 15% 10% 8% 1% 1% 1% 1%
2 15% 61% 9% 10% 1% 1% 1% 1%
3 28% 23% 38% 4% 3% 3% 0% 1%
4 22% 29% 4% 39% 0% 0% 2% 3%
5 26% 32% 20% 4% 15% 2% 2% 0%
6 34% 24% 25% 3% 2% 11% 1% 0%
7 35% 24% 4% 22% 1% 1% 11% 2%
8 20% 34% 6% 25% 1% 0% 3% 11%
1 2 3 4 5 6 7 8
1 0.9 0.8 0.7 0.6 0.5 0.4 0.3 0.2 0.1 0
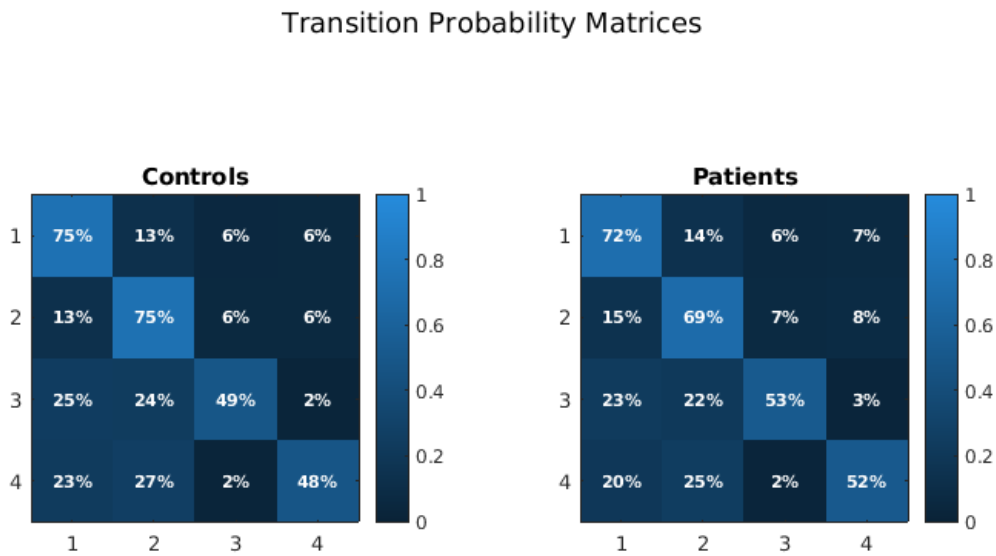
Bottom DMN+DAN